CLM-FruitTree: A new sub-model for deciduous fruit trees in the Community Land Model (CLM5)

Olga Dombrowski[1], Cosimo Brogi[1], Harrie-Jan Hendricks Franssen[1], Damiano Zanotelli[2], Heye Bogena[1]

[1]Agrosphere (IBG-3), Forschungszentrum Jülich GmbH, Jülich, 52425, Germany
5 [2]Faculty of Science and Technology, Free University of Bolzano, Bolzano, 39100, Italy

Correspondence to: Olga Dombrowski (o.dombrowski@fz-juelich.de)

Abstract. The inclusion of perennial, woody crops in land surface models is crucial to address their role in carbon (C) sequestration, food production, and water requirements under climate change. To help quantifying the biogeochemical and biogeophysical processes associated with these agro-ecosystems, we developed and tested a new sub-model, CLM-FruitTree, 10 for deciduous fruit orchards within the framework of the Community Land Model version 5 (CLM5). The model development included (1) a new perennial crop phenology description, (2) an adapted C and nitrogen allocation scheme, considering both storage and photosynthetic growth of annual and perennial plant organs, (3) typical management practices associated with fruit orchards, and (4) the parameterization of an apple plant functional type. CLM-FruitTree was tested using extensive field measurements from an apple orchard in South Tyrol, Italy. Growth and partitioning of biomass to the individual plant 15 components was well represented by CLM-FruitTree and average yield was predicted within 2.3 % of the observed values despite low simulated inter-annual variability compared to observations. The simulated seasonal course of C, energy, and water fluxes was in good agreement with the EC measurements owing to the accurate representation of the prolonged growing season and typical leaf area development of the orchard. We found that gross primary production, net radiation, and latent heat flux were highly correlated (r > 0.94) with EC measurements and showed little bias (< ±5 %). Simulated respiration components, 20 sensible heat, and ground heat flux were less consistent with observations. This was attributed to simplifications in the orchard structure and to the presence of additional management practices that are not yet represented in CLM-FruitTree. Finally, the results suggested that the representation of microbial and autotrophic respiration, and energy partitioning in complex, heterogeneous canopies in CLM5 requires further attention. The new sub-model CLM-FruitTree improved the representation of agricultural systems in CLM5 and can be used to study land surface processes in fruit orchards at the local, regional or 25 larger scale.

1 Introduction

Orchards and other perennial fruit crops are a major component of the global agricultural production with significant coverage

30   and yield in China, the United States, south-western Africa, and some parts of Europe (Fao, 2021). In the European region, perennial crops are a key economic element of Mediterranean agro-ecosystems as they provide 45 % of the local agricultural output (Lobianco and Roberto, 2006). Apples are the most important fruit tree crop as one third of European orchards is devoted to their production. With a coverage of 984'509 ha, they provide a yearly harvest of over 17 million tons which is one fifth of the overall European fruit production in terms of output value (Fao, 2021).

35   In contrast to annual crops, fruit trees can be productive for several decades before rotation is needed. Their prolonged growing season, standing biomass, and low respiratory losses can support carbon (C) storage and promote higher carbon use efficiencies (Wünsche and Lakso, 2000; Zanotelli et al., 2013). The transport of C stored in biomass into the soil in addition to reduced soil tillage and disturbances under fruit orchards compared to annual crops further promote C sequestration (Bwalya, 2012; Wu et al., 2012; Ledo et al., 2020). The FAO has therefore suggested perennial agriculture as a possible measure to mitigate

40   climate change and enhance food security (Glover et al., 2010), and many studies have recently investigated this potential for various fruit orchards (Wu et al., 2012; Scandellari et al., 2016; Hammad et al., 2020; Yasin et al., 2021). The study of water and irrigation requirements in fruit orchards has become another field of intense research due to the need for a more resilient agriculture in the context of climate change and water supply shortages (Maestre-Valero et al., 2017; El Jaouhari et al., 2018; O'connell and Scalisi, 2019; Segovia-Cardozo et al., 2022). In order to answer questions related to C sequestration, water

45   requirements, and sustainable food production of fruit orchards, a better understanding of the related ecosystem processes is vital (Fader et al., 2015).

Models with a comprehensive description of the carbon, water, and energy fluxes, such as global land surface models (LSMs), are a powerful tool to explore complex ecosystems like the abovementioned fruit orchards. The use of LSMs was recently extended to not only model the processes at the land–atmosphere interface, but also to study the response of ecosystems and

50   water resources to climate change (Prentice et al., 2015; Fisher and Koven, 2020; Blyth et al., 2021). To quantify these effects, LSMs need to represent a wide range of land use and vegetation types. However, most LSMs consider only perennials such as deciduous and coniferous trees, as well as major annual crops such as wheat, soy, or maize (Lawrence et al., 2018). Recently, some LSMs additionally include bioenergy crops (Schaphoff et al., 2018), while others group crops into a few generic crop types (Noilhan and Mahfouf, 1996; Krinner et al., 2005; Balsamo et al., 2009). Despite their significance, perennial crops,

55   such as fruit trees, are rarely considered in LSMs and attempts of including them in global and regional modelling environments are scarce (Fader et al., 2015; Cheng et al., 2020). An example of such an attempt is the inclusion of agricultural trees (e.g., grapes, cotton, and apple trees) in the Lund-Potsdam-Jena managed Land model to improve the representation of Mediterranean agro-ecosystems (Fader et al., 2015). Here, agricultural trees were modelled as small trees and fruit harvest was determined as the product of a plant specific harvest index and the net primary productivity (NPP). Other authors parameterized

60   oil palm trees, a perennial evergreen crop, in the Community Land Model (CLM) version 4.5 (Fan et al., 2015). Palm trees

were represented by a new phenology where large palm leaves with fruit bunches emerge successively, leaves are pruned regularly, and harvest occurs once a month. Recently, two perennial grasses for energy production were parameterized in the latest version of the model, CLM5 (Cheng et al., 2020). Parameters for bioenergy crops were tuned using sensitivity analysis and observations, while harvest was represented by removing around 70 % of the aboveground biomass.

65 While the above-mentioned studies describe some common features of perennial plants, they do not, or only partially, represent the seasonal deciduous phenology of fruit trees or the explicit modelling of fruit growth. Furthermore, key aspects such as C reserve deposition and mobilization in the following spring are generally not considered, possibly due to necessary simplifications or because the drivers of these processes are still not fully understood (Le Roux et al., 2001; Neumann, 2020). The absence of perennial crops in land surface models introduces a significant bias in the representation of biogeophysical and

70 biogeochemical processes in agro-ecosystems where this type of cultivation is prevalent. As a result, the response to climate change in terms of C sequestration, water requirements, or food production cannot be assessed adequately in regions such as the Mediterranean, where perennial, woody crops are very common and play a vital role for food security and economy (Fader et al., 2015; Lobianco and Roberto, 2006).

Although deciduous fruit trees share certain characteristics with natural vegetation and annual crops in LSMs such as CLM5,

75 several particularities in their growth dynamics and management practices still prevent a meaningful simulation using currently available representations of vegetation. In this study, we therefore provide CLM5 with the ability of modelling perennial fruit trees and the associated processes. For this purpose, we developed a new sub-model named CLM-FruitTree within the existing model framework of CLM5. CLM-FruitTree combines elements of the broadleaf deciduous tree subroutine such as growth and C turnover of woody components, with distinctive phenological stages and a harvestable organ similar to the annual crop

80 subroutine. We first describe the model conceptualization including the new phenology, carbon and nitrogen (CN) allocation, and management options. We further demonstrate the applicability of CLM-FruitTree by parameterizing a new apple plant functional type (PFT). Finally we evaluate and discuss the model performance using extensive field data from an apple orchard in South Tyrol, Italy.

2 Methods

85 ### 2.1 Vegetation characterizations in CLM5

The latest version of the Community Land Model, CLM5, simulates the exchange of water, energy, C, and nitrogen (N) between land and atmosphere as well as their storage and transport on the land surface and in the subsurface, driven by climate variability and modulated by soil and vegetation states and characteristics. The land surface in CLM5 is characterized by one of five land units namely glacier, lake, urban, vegetated, and crop. These units are further divided to capture the variability in

90 soil, vegetation, and management options (i.e., irrigated or non-irrigated). Compared to previous model versions, CLM5 features various improvements in the representation of land use and vegetation modelling such as plant CN cycling, soil and plant hydrology and crop modelling (Lawrence et al., 2018).

The inclusion of the Biome-BGC (Biome BioGeochemical Cycles) model into CLM4 allowed the simulation of 15 different PFTs of natural, woody and non-woody, vegetation including broadleaf deciduous trees (BDT). The latter is described by an

95 algorithm for the seasonal phenology of deciduous trees that controls changes in phenology, as well as the C and N fluxes between different plant and litter pools. Here, leaf onset and offset periods mark the beginning and end of a growing season. Once a new onset growth period is initiated, C and corresponding N fluxes occur out of a storage pool into a transfer pool (intermediate pool to separate fluxes in and out of the storage pool) from where they are gradually transferred to the displayed growth pool (Fig. 1). All plant organs are maintained separately in each of the three pools. During the active growth period, C

100 and corresponding N storage pools of the individual plant organs are replenished based on fixed stoichiometric relationships and C:N ratios of each plant organ. At leaf offset, C and N pools feed the litter or coarse woody debris pool, while others are retained as structural woody tissue.

In addition, CLM5 now features the Biogeochemistry Crop Module (BGC-crop), adopted from the prognostic crop module of the Agro-Ecosystem Integrated Biosphere Simulator (Agro-IBIS), which provides eight different annual crop species with

105 interactive crop management options (i.e., irrigation and fertilization). Another 23 currently inactive crop types can be defined but have not been provided with specific crop parameters. Crop phenology and CN allocation follow three phenological phases: (1) from planting to leaf emergence, (2) from leaf emergence to the start of grain fill, and (3) from grain fill to grain maturity and harvest, that are controlled by temperature and growing degree-day (GDD) thresholds. Different to natural vegetation, all assimilates are directed to the displayed pools while the storage pools remain unused. At harvest, C and N from the grain pool

110 are transferred to a grain product pool while a small amount is kept to reseed the crop in the following year. All remaining plant parts feed the litter cycle (Fig. 1). The reader is referred to the technical documentation of CLM5 for a more detailed description of the vegetation and crop description (Lawrence et al., 2018).

From the above description of the existing model components, the following limitations for the application of CLM5 to deciduous fruit trees arise: (1) the current CLM-BGC-crop algorithm does not allow the simulation of perennial and/or woody

115 crops; (2) the seasonal deciduous phenology algorithm although describing some characteristics common to fruit trees, lacks the capability of simulating a harvestable organ, independent development of different plant parts, and active growth in the current season; (3) typical management practices of fruit orchards such as transplanting of tree seedlings and pruning are currently not represented in CLM5; and (4) there is no parameterized fruit tree PFT in the default parameter set of CLM5.

2.2 Model conceptualization

120 To resolve the model limitations discussed in Sect. 2.1, we have developed a new sub-model CLM-FruitTree to model growth and yield of deciduous fruit trees grown in orchard systems as well as the associated ecosystem processes. More specifically, for the implementation of CLM-FruitTree, we introduced a new phenology subroutine including crop management options next to the existing subroutines of natural vegetation and crops. In addition, the CN allocation module as well as corresponding modules (including C and N state and flux updates, vegetation structure, and respiration) were modified. The modification of

125 sub-routines and creation of new parameters followed CLM5 standards and the given model structure. Where necessary, new

history and restart variables were added to restart simulations with bit-for-bit continuity of the output (Lawrence et al., 2018). Furthermore, to test the new sub-model, an apple PFT was parameterized and added to the active crops using one of the existing but currently inactive crop types in CLM5, type 35 and 36 (rain fed and irrigated citrus).

CLM-FruitTree combines characteristics of both BDT and annual crops to simulate a perennial woody crop with a harvestable
130 organ (Fig. 1). Similar to the existing BDT phenology algorithm in CLM5, the fruit tree algorithm uses a perennial deciduous phenology with standing woody biomass and annual leaf shedding. During the active growth period however, the phenology and CN allocation of vegetative and harvestable organs are described by distinct growth phases and are driven by a GDD summation similar to the crop phenology.

An orchard is established by transplanting small tree seedlings from nursery, a typical planting method for this type of
135 cultivation (Wheaton et al., 1990; Corelli-Grappadelli and Marini, 2008). Once planted, the orchard remains productive for 25–40 years as defined by the user. In CLM-FruitTree, both stored C and current photosynthesis contribute to growth of the fruit tree, as leaf and shoot development at the beginning of a growing season utilize carbohydrate reserves and nitrogenous compounds that were accumulated during the previous season (Tromp, 1983; Oliveira and Priestley, 1988; Loescher et al., 1990). Deciduous fruit trees are dormant in winter and resume growth in spring after meeting species- and cultivar-specific
140 chilling and heat requirements (Anderson et al., 1985; Faust et al., 1997; Zavalloni et al., 2006), which is represented in CLM-FruitTree using the chilling and forcing model suggested by Cesaraccio et al. (2004). Early in the season, the canopy develops rapidly until it reaches maturity typically by midsummer, while leaf shedding occurs when temperatures drop in autumn (Kozlowski, 1992; Loescher et al., 1990; Lakso et al., 1999). Fruit trees usually start flowering 3–4 weeks after bud burst, which is not specifically represented by CLM-FruitTree which instead assumes that fruit growth begins after full bloom (Lakso
145 et al., 1999). Fruit growth is described by two stages, cell division and cell expansion that together form a sigmoid growth curve for many fruit tree species such as apple, pear, and orange (Corelli-Grappadelli and Lakso, 2002; Jackson, 2011).

In the following, the new developments to account for the distinct phenology, CN allocation, and management practices of a fruit orchard are described in more detail. Other biochemical and biophysical processes such as photosynthesis, water and litter cycles, and fixation and uptake of N were not modified except for minor adaptations to the retranslocation of N and respiration.
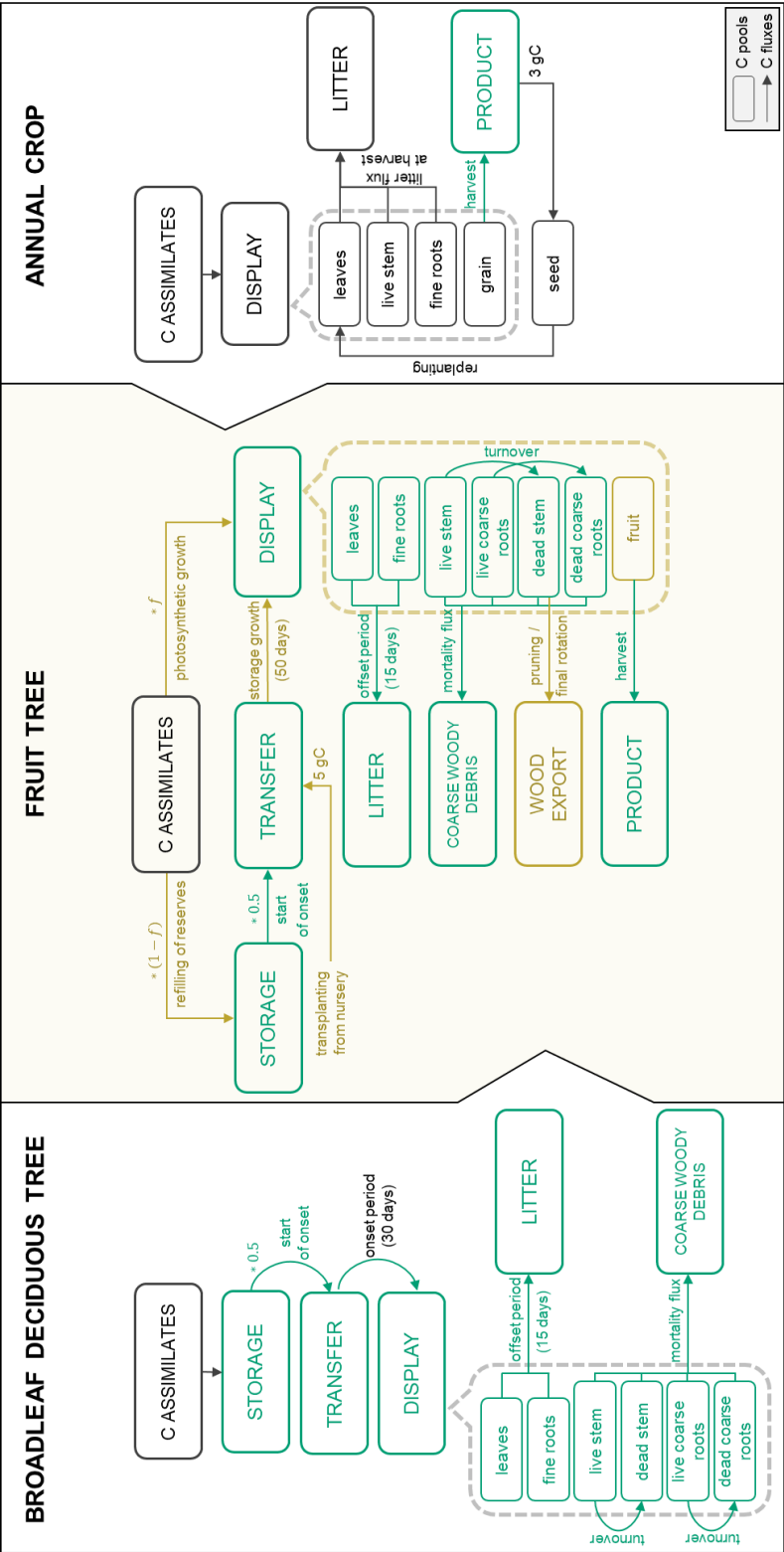
Figure 1: Schematic of the main phenology and C allocation features of the broadleaf deciduous tree and annual crop representations in CLM5 as well as the new sub-model CLM-FruitTree. C pools within the dashed boxes are the individual components that make up the displayed C pool (the same components can be found for storage and transfer pools respectively). Carbon pools and fluxes in green were reused for CLM-FruitTree while pools and fluxes in ochre were modified or newly added.

Geoscientific
Model Development
Discussions

2.2.1 Phenology

A new orchard lifecycle is initialized by transplanting seedlings at the beginning of the year during dormancy. An initial biomass of 5 gC m^{-2} is assigned to leaf and fine root transfer pools, and 0.5 gC m^{-2} is assigned to the dead stem pool. Each pool is also assigned the corresponding amount of N. Apple growth thereafter is described by six post-planting phenological stages, namely: (1) bud break, (2) fruit growth, (3) fruit ripening, (4) canopy maturity, (5) fruit maturity and harvest, and (6) start of leaf senescence (Fig. 2).

Bud break is predicted by a sequential model that first accumulates chill days followed by anti-chill days based on a predefined temperature threshold and chilling requirement (Cesaraccio et al., 2004). More information on the sequential model and the calibration of model parameters can be found in Appendix A. At bud break, a portion of the C in the storage pool of all plant components, except fruits, is transferred to the actively growing C pools over a period of 50 days as controlled by the newly added parameter *ndays_stor*. Outside the dormant period, leaf and fruit development occur independently as fruit growth typically starts 4–5 weeks after bud break while canopy development continues until mid-season and leaf senescence does not occur until after the fruits are harvested (Wünsche and Lakso, 2000; Goldschmidt and Lakso, 2005) (Fig. 2).

The thermal thresholds to reach phases (2)–(5) (Appendix C) are defined as accumulated GDDs since bud break. GDDs are determined as the difference between the average daily air temperature and a base temperature of 4 °C with a maximum daily increment of 26 °days (Eq. (1)). Different to the existing deciduous phenology, leaf senescence is triggered not by day length but by the drop of the daily mean temperature below a critical temperature threshold, in this case the base temperature. This approach was selected since many fruit trees that belong to the Rosaceae family (e.g., apple, pear, plum, and cherry) are unaffected by photoperiod and instead controlled by temperature (Heide and Prestrud, 2005). The last day of the leaf-offset period marks the beginning of dormancy. The new phenology subroutine of CLM-FruitTree also controls C reserve dynamics, stem and root turnover, and final rotation, which involves removing and replanting trees when the maximum orchard lifespan is reached.
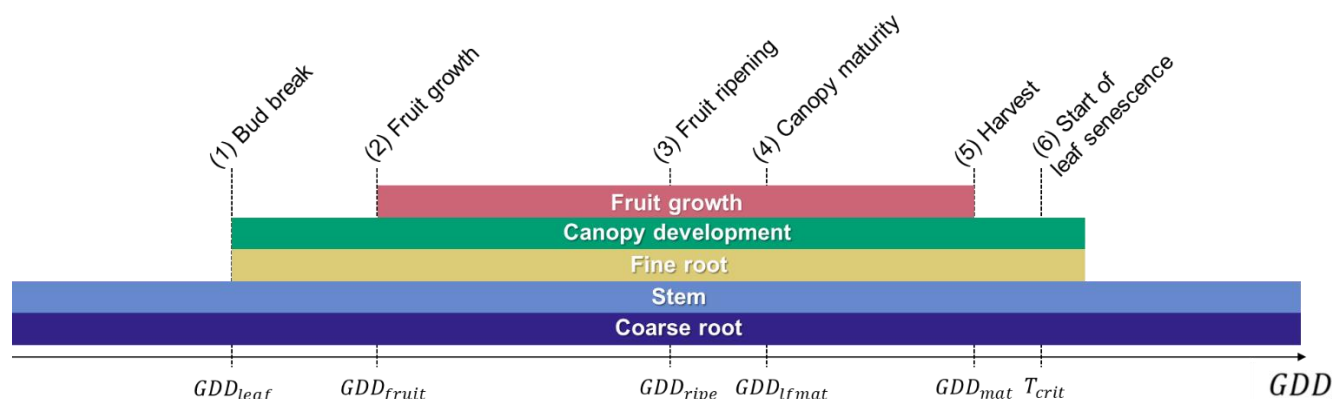

Figure 2: Fruit tree phenological stages of (1) bud break at the end of dormancy, (2) the start of fruit growth, (3) fruit ripening, (4) canopy maturity, (5) harvest, and (6) the start of leaf senescence. The lengths of phenological stages (2)-(5) are determined by their

180 **respective growing degree-day thresholds (GDD) starting from bud break (GDD$_{leaf}$=0), while stage (6) is determined by a critical temperature threshold (T$_{crit}$).**

2.2.2 Carbon and nitrogen allocation

CN allocation to the growth of new tissue (display pools) and to storage pools follows the phenological stages described in Sect. 2.2.1 (Fig. 2). A coupled CN allocation subroutine determines the fate of newly assimilated C from photosynthesis. The

185 potential allocation to the different plant components is based on allocation coefficients and allometric relationships between dead and alive parts of stem and coarse root. Throughout the growing period until harvest, 5 % of the newly assimilated C is allocated to the storage pools, as defined by the *fcur* parameter. The remainder is allocated to the displayed C pools except for fruits where all allocated C is assigned to the displayed pool.

Before the start of fruit growth, phase (1), available C and N are partitioned between leaves, stem and root pools. The allocation

190 coefficients are calculated according to a set of equations that were adapted from the AgroIBIS crop phenology algorithm used in CLM5-BGC-crop (Lawrence et al., 2018):

$$GDD_{T2m} = GDD_{T2m} + T_{2m} - T_f - 4 \qquad \text{where} \quad 0 \le T_{2m} - T_f - 4 \le 26 \,°days \,, \tag{1}$$

$$a_{repr} = 0 \,, \tag{2}$$

$$a_{froot} = a_{froot}^i - \left(a_{froot}^i - a_{froot}^f\right) * \frac{GDD_{T2m} - GDD_{leaf}}{GDD_{fruit} - GDD_{leaf}} \,, \tag{3}$$

$$a_{leaf} = \left(1 - a_{froot}\right) * \frac{a_{leaf}^i * (e^{-b} - e^{-b * \frac{GDD_{T2m} - GDD_{leaf}}{GDD_{lfmat} - GDD_{leaf}}})}{e^{-b} - 1} \,, \tag{4}$$

$$a_{livestem} = 1 - a_{repr} - a_{froot} - a_{leaf} \,, \tag{5}$$

where GDD_{T2m} are the accumulated growing degree-days for the 2-m air temperature with maximum increments of 26 °days; T_{2m} is the simulated 2-m air temperature in K; T_f is the freezing temperature of water and equals 273.15 K; GDD_{leaf},

195 GDD_{fruit}, and GDD_{lfmat} are thermal thresholds for bud break, start of fruit growth, and canopy maturity, respectively; b is an exponential factor; a_{leaf}^i, a_{froot}^i, and a_{froot}^f are initial and final values for the allocation coefficients to leaf (a_{leaf}) and fine root (a_{froot}), respectively; and a_{repr} and $a_{livestem}$ are the allocation coefficients to fruit and live stem, respectively.

Once fruit growth begins in phase (2), an increasing proportion of the assimilated C is allocated to this organ, causing leaf allocation to decline and fruit allocation to plateau at a high value once canopy maturity is reached. Fine roots and stem
200 continue to decline and then settle at a constant value until harvest.

$$a_{livestem} = a_{livestem} * \left(1 - \frac{(GDD_{T2m}-GDD_{leaf})-(GDD_{fruit}-GDD_{leaf})}{(GDD_{mat}-GDD_{leaf})^{d_L-(GDD_{fruit}-GDD_{leaf})}} \right)^{d_{alloc}^{stem}},$$ (6)

$$a_{repr} = 1 - a_{froot} - a_{livestem} - a_{leaf},$$ (7)

where GDD_{mat} is the thermal threshold for fruit maturity and harvest, while d_L and d_{alloc}^{stem} are stem allocation decline factors.

After harvest and until the start of dormancy, all of the newly assimilated C is sent to the storage pools following the notion that late in the season, assimilates are used mostly to fill up reserves that can be mobilized to resume growth in the following spring (Le Roux et al., 2001). Fruit trees store C in the perennial woody parts of the tree from where it is remobilized to support
205 the growth of new shoots, leaves, and fine roots (Oliveira and Priestley, 1988; Millard, 1996; Le Roux et al., 2001). Since in CLM5 separate storage pools are assigned to each plant organ, the newly added *aleafstor* parameter (Table C1) defines the fraction of allocatable C going to the leaf storage pool while the remainder is split equally between roots and stem.

2.2.3 Parameterization of other processes and management practices

210 Fruit trees, similar to other deciduous species, have been observed to translocate N out of senescent leaves to be reused by other tree organs (Murneek, 1942; Bollard, 1960). Therefore, CLM-FruitTree adopts the same N retranslocation strategy as used in the BDT phenology (Lawrence et al., 2018). Furthermore, management practices such as fertilization and stem pruning are represented in the new sub-model. Fertilization is performed on a yearly basis after the occurrence of bud break, as N fertilization in early spring is still the most common practice in fruit orchards even though autumn fertilization or multiple
215 applications via fertigation are also in use to increase fertilizer N use efficiency and reduce N losses (Sanchez et al., 1995; Carranca et al., 2018). We use the existing fertilization scheme of the crop phenology that adds fertilizer directly to the soil mineral N pool. A user-defined fertilization rate or amount can be applied as synthetic fertilizer or manure respectively, although there currently is no difference in model behaviour for these two fertilizer types (Lawrence et al., 2018).
Pruning is performed as the tree enters dormancy by removing a user-defined fraction, *prune_fr* (Table C1), of the dead stem
220 from both storage and displayed C pools. Pruning residues are treated in one of two ways: (1) residues are added to the wood harvest pool and exported from the field or (2) residues are mulched into the soil thus feeding the litter cycle. The former is typically adopted in conventional agriculture were residues are exported and treated as waste (Benyei et al., 2018) or utilized for energy production (Kazimierski et al., 2021). The latter is more common in orchards under organic production to increase C sequestration in soils (Montanaro et al., 2010; Aguilera et al., 2015). During the first three years after planting, trees are not
225 pruned to allow some initial stem biomass to grow. In practice, winter pruning in fruit orchards may be performed throughout

the winter to control the shape and size of fruit trees, and partially to manage crop load (Grechi et al., 2008). The pruning implemented in CLM-FruitTree affects only the dead stem biomass and tree height that is calculated based on this biomass pool, which in turn effects the calculation of turbulent fluxes of sensible and latent heat. However, this effect is small, and since turbulent fluxes are generally low in winter, the exact timing of pruning does not play a significant role in the magnitude

230 of these fluxes. When the orchard reaches the end of its lifespan, C of all biomass pools (storage, transfer, and display) is sent to either the litter pool for leaves and fine roots, or the wood harvest pool for live and dead stem and coarse roots while any remaining C in the fruit pool is harvested. The orchard can then be replanted in the following year. Lastly, the standard irrigation routine implemented in CLM5 can be used for irrigated orchards by selecting the irrigated crop PFT.

2.3 Model implementation and testing

235 ### 2.3.1 Site data

Extensive field measurements from an apple-growing region in the Adige River valley, South Tyrol, Italy (46°21' N, 11°16' E; 240 m a.s.l.) were used to parameterize and test the new sub-model CLM-FruitTree along with the new apple PFT (Zanotelli et al., 2013; Zanotelli et al., 2015; Zanotelli et al., 2019). Measurements were obtained from an approximately 0.5 ha irrigated apple orchard planted in 2000 with the Fuji apple cultivar grafted on M9 dwarfing rootstock. The apple trees were planted at

240 a row and tree spacing of 3x1 m (3333 trees ha^{-1}). A 1.8 m wide grass strip was grown between the tree rows, which was mowed 3 times a year. Other management practices included regular pruning, spring fertilization of 7.5 gN m^{-2} yr^{-1}, and tillage of the soil directly underneath the trees (Zanotelli et al., 2013). Stand-related data included general stand characteristics and phenology observations, leaf area index, C:N ratios, rooting distribution at three depth ranges (0–20 cm, 20–40 cm, and 40–60 cm), measurements of the biomass growth of different tree organs at monthly or seasonal interval, and fruit harvest

245 information (Table 1). Furthermore, daily soil respiration measurements from a control and a trenching plot (with (R_s) and without root respiration (R_h), respectively) were performed in 2010. Additionally, an eddy covariance (EC) station provided measurements of the turbulent exchange of trace gases and energy at the studied apple orchard between 2013 and 2015. The quality check, gap filling, and flux partitioning of collected data followed the procedure outlined in Reichstein et al. (2005). The average closure of the energy balance was 60 %. To correct for the closure failure, the missing energy was assigned to the

250 latent (LE) and sensible (H) heat fluxes based on the daily Bowen ratio (Zanotelli et al., 2019). Measured or derived fluxes included net ecosystem CO_2 exchange (NEE), ecosystem respiration (R_{eco}), gross primary production (GPP), LE, H, and evapotranspiration (ET) at half-hourly intervals. Furthermore, soil heat flux (G) measured at 5cm depth as well as soil moisture measurements up to a depth of 60 cm of soil are available. Table 1 gives a summary of the available data and measurement periods. A complete description of the measurement procedures and instruments can be found in Zanotelli et al. (2013),

255 Zanotelli et al. (2015), and Zanotelli et al. (2019).

Meteorological data, recorded partly at the EC tower and at the Laimburg meteorological station located 4 km from the site (46°23' N, 11°17' E; 224 m a.s.l.), were used at an hourly time step to force the model. Measured data included precipitation,

solar radiation, net radiation (R_n, only at EC tower), air temperature, air pressure (only at Laimburg), relative humidity, and wind speed. Measurements of incoming longwave radiation (LW_{in}) were available for 2010 only, but additional calculations

260 following Konzelmann et al. (1994) and Sedlar and Hock (2009) were produced and used as forcing for the remaining years 2011–2019 (Appendix B). This was necessary since the use of the internally calculated LW_{in} in CLM5 resulted in unrealistic underestimations compared to the available measurements of LW_{in} leading to a significant bias in R_n.

Table 1: Summary of available data from an apple orchard in the Adige River valley, South Tyrol, Italy between 2010 and 2019. Solid lines represent continuous, dotted lines monthly measurements, and diamonds represent single measurements.

Data	2010	2011	2012	2013	2014	2015	2016	2017	2018	2019
Weather data EC tower	▬		▬	▬	▬	▬				
Weather data Laimburg	▬	▬	▬	▬	▬	▬	▬	▬	▬	▬
Biomass (NPP) components	⋯	◆	◆							
C:N ratios of biomass components	⋯									
Leaf area index (LAI)	⋯⋯⋯⋯									
Fruit production (yield)		◆	◆	◆	◆	◆	◆			
Root distribution (0–60 cm)	◆									
Soil respiration (R_s, R_h)	▬									
Soil heat flux (G)				▬	▬	▬				
Soil water content (SWC, 0–60 cm)				▬	▬	▬				
EC data: carbon (GPP, R_{eco}, NEE), energy (R_n, LE, H), water (ET)				▬	▬	▬				

2.3.2 Model setup

The model was set up in point mode to simulate the apple orchard in the Adige valley using available sand, clay, and organic matter fractions. The model was spun-up for 200 years, first in accelerated decomposition and then in normal decomposition mode, until all state variables, such as total ecosystem soil C and soil water, reached equilibrium (Lawrence et al., 2018). For

270 the model spin-up, the CRUNCEPv7 atmospheric forcing data set from 1986 to 2016 was used (Viovy, 2018). The apple orchard was then initiated using the newly developed sub-model and the apple PFT selecting the site-specific management (i.e., fertilization with 7.5 gN m^{-2} yr^{-1}, irrigation, mulching of pruning material). Simulations were performed for a period of 10 years to mirror the time from orchard establishment in 2000 up to the start of the measurements in 2010 using 10 years (2010–2019) of the available meteorological data from Laimburg meteorological station. Simulations were then extended for

275 another 6 years from 2010 to 2015 for model parameterization and performance evaluation purposes.

2.3.3 Parameterization

Key parameters of the new sub-model as well as other PFT-specific parameters were parameterized using the first 3 years of simulations between 2010 and 2012. The length of phenological stages and associated parameters were determined based on field observations of bud burst, full bloom, and harvest as well as non-cultivar specific apple phenology descriptions that were

280 found in the literature (Appendix C). C allocation coefficients were calculated based on the monthly measurements in 2010, by dividing the biomass growth of the individual plant organs by the total biomass increment. Subsequently, model parameters associated with the CN allocation subroutine (Eq. (2) – (7)) were calibrated manually to match the coefficients obtained from the observations and the overall biomass partitioning on a yearly basis. Parameter values for C:N ratios of all plant organs and maximum LAI were based on field observations in 2010 and 2010–2012, respectively. The specific leaf area index was

285 calculated by dividing monthly measurements of LAI by leaf biomass and taking the average of the obtained values. Plant morphological parameters such as maximum tree height, stocking density, or rooting depth were adjusted based on site-specific information. The CLM5 root distribution parameter, which sets the root ratios at different depths, was calibrated by least squares regression of the measured root ratios at 0–20 cm, 20–40 cm, and 40–60 cm depths and the calculated ratios. Optical parameters for leaf transmittance and reflectance in the visible and near-IR were set to average values reported for apple by

290 Bastías and Corelli-Grappadelli (2012). Stem reflectance and transmittance were assumed to be similar to other woody species and therefore set to the values used for BDT in CLM5, similar to the assumptions made by Fan et al. (2015) for the palm tree development in CLM4.5. The ratio of momentum roughness length to canopy top height was set to the average value of the ranges reported for apple and citrus orchards (Tanny and Cohen, 2003; La Fuente-Sáiz et al., 2017). No specific values could be found for the ratio of displacement to top of canopy height, the leaf orientation index, or the intercept to calculate the top

295 of canopy maintenance respiration base rate. These values were assumed to be comparable to other deciduous trees and thus set to the values used for BDT in CLM5. Parameters related to C reserve dynamics (e.g., *fcur*) and photosynthesis (e.g., the slope of the relationship between leaf N per unit area and the maximum rate of carboxylation at 25 °C) were adjusted to match observed LAI and productivity data. All parameters with their values and references to the literature are summarized in Table C1 of the Appendix.

300 2.3.4 Sensitivity Analysis

A simple one-by-one sensitivity analysis was performed to further tune model parameters and assess the influence of newly added parameters on the simulations. As a complete sensitivity analysis of all PFT-related parameters would have exceeded the scope of this study, the analysis focused on key parameters of the new phenology and CN allocation subroutines. Other potentially influential parameters were selected based on previously performed sensitivity analyses by Göhler et al. (2013) for

305 CLM3.5, and by Cheng et al. (2020) and Dagon et al. (2020) for CLM5 taking into account differences between previous and current model versions. Parameters selected for the analysis were perturbed by varying a parameter by ±30 %, ±20 %, and ±10 % while keeping the others fixed to the value of the control simulation (after initial parameterization). The goal here was not

to perform an in-depth analysis covering the full range of possible parameter values, but rather to provide a first indication of influential parameters in the new sub-model similar to the approach of Fan et al. (2015). As a measure of sensitivity, the

310   parameter effect (PE) was calculated using the average of 3 years of simulations between 2013 and 2015 of the control and the perturbed simulations for selected output variables and the following formula adjusted from Luo et al. (2020):

$$\Delta X_{i,j} = \sum_{k=1}^{n} \frac{\left|\overline{X_{i,j,k}} - \overline{X_{i,control}}\right|}{\left|\overline{X_{i,control}}\right|} \ , \tag{8}$$

$$PE_{i,j} = \frac{\Delta X_{i,j}}{max\left[\left(\Delta X_{i,j}\right)_{1\leq i\leq n;1\leq j\leq m}\right]} \ , \tag{9}$$

where k is the parameter perturbation factor, i is the ith variable across $n = 6$ selected output variables including: GPP, NEE, R_a, LE, maximum LAI, and yield, j is the jth parameter across m selected parameters. $PE_{i,j}$ is a number between 0 and 1 that

315   represents the sensitivity of an output variable i to the parameter j, with 1 meaning high and 0 meaning low sensitivity. The parameters selected for sensitivity analysis are indicated in Table C1 of the Appendix.

2.3.5 Model performance evaluation

Modelling results are compared to observed biomass, yield, and LAI data as well as ecosystem fluxes retrieved from the EC measurements. Statistical indices for model performance evaluation include the Pearson's coefficient of correlation (r), the

320   root mean square error (RMSE) and the percent bias error (%bias):

$$r = \frac{\left(\frac{1}{n}\sum_{i=1}^{n}(X_i^o - \mu^o)*(X_i - \mu)\right)}{\sigma * \sigma^o} \ , \tag{10}$$

$$RMSE = \sqrt{\frac{1}{n}\sum_{i=1}^{n}(X_i - X_i^o)^2} \ , \tag{11}$$

$$\%bias = \frac{\sum_{i=1}^{n}(X_i - X_i^o)}{\sum_{i=1}^{n}(X_i^o)} \ , \tag{12}$$

where i is the time step, n is the total number of time steps, and X_i and X_i^o are simulated and observed values at each time step respectively, μ and μ^o are simulated and observed mean values, respectively, and σ and σ^o are simulated and observed standard deviations.

325

3 Results and discussion

3.1 Sensitivity analysis

A total of 34 parameters were initially considered for the sensitivity analysis of which the 13 most influential parameters (PE > 0.1 for at least one of the selected output variables) are shown in Fig. 3. GPP, NEE, R_a, and yield have similar sensitivity

330 patterns and are most sensitive to the leaf C:N ratio (*leafcn*) and the relationship between leaf N and the maximum rate of carboxylation at 25 °C (*s_vcad*). Together with the specific leaf area (*slatop*) and other constants, they control the maximum photosynthetic capacity in the photosynthesis calculation and thus largely influence total C assimilation. As expected, LAI is most influenced by parameters that control the CN allocation to leaves such as the initial leaf allocation coefficient (*fleafi*), the GDDs needed to reach canopy maturity (*lfmat*), the maximum LAI (*laimx*), photosynthetic parameters, and, to a smaller extent,

335 the fraction of C allocated to the leaf storage pool to refill C reserves (*aleafstor*). The first three parameters influence leaf biomass and thus show a considerable effect on GPP, NEE, R_a, and yield. The same output variables are affected in a similar fashion by the GDDs needed until fruit harvest (*hybgdd*) that control the amount of C allocated to fruits. LE is influenced largely by the parameter controlling stomatal conductance (*medlynslope*), and the photosynthetic parameters (*leafcn*, *s_vcad*). Overall, photosynthetic parameters play a key role in determining the magnitude of the studied output variables with an average

340 PE value close to 0.7 across all six variables. Phenological parameters (top seven parameters in Fig. 3) are generally less influential for the same output variables with average PE values up to 0.43. These findings are largely consistent with earlier studies of parameter sensitivity (Göhler et al., 2013; Cheng et al., 2020; Dagon et al., 2020; Luo et al., 2020). In contrast to Luo et al. (2020) we did not find a strong effect of the root distribution parameter (*rootprof_beta*) on LE, which can be attributed to the low water stress due to the irrigation management of the studied orchard.

345 While the one-at-a-time sensitivity analysis provides some insight into model sensitivity, the ranking of influential parameters is strongly influenced by the choice of parameters and output variables, the parameter perturbation strategy (i.e. percent change, linear sampling), and the index chosen as the sensitivity measure. Parameter tuning based on this analysis is further complicated since this approach does not consider parameter covariation that is particularly strong for plant parameters that influence photosynthesis (Göhler et al., 2013). Selecting parameter values based on the individual best simulation hence does not

350 necessarily yield the best overall result (Luo et al., 2020). We therefore decided to first adjust *s_vcad* to best match the observed average GPP. In the following, we further adjusted *fleafi*, *hybgdd* and *medlynslope* to improve the simulated biomass components as well as the LE flux, respectively.
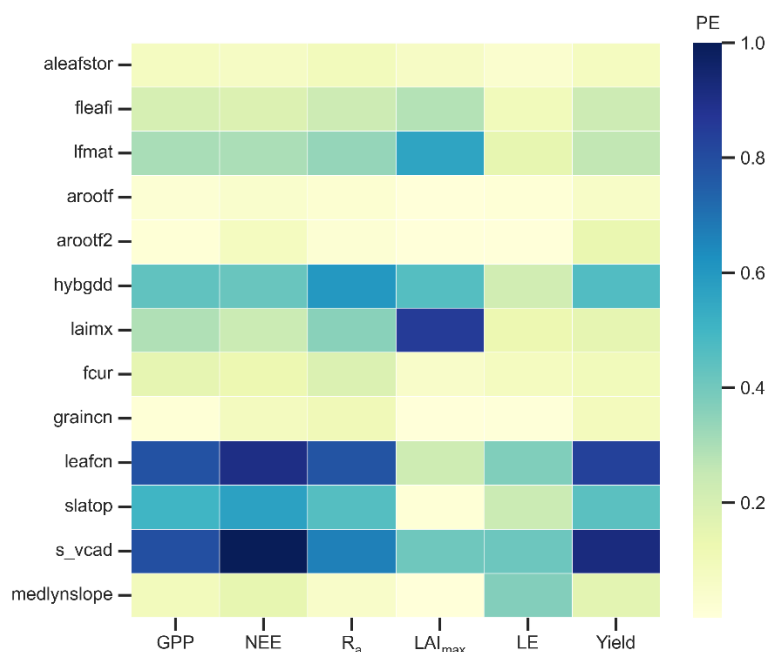
14

Figure 3: Parameter effect (PE) as a measure of sensitivity of selected output variables to the most influential model parameters.
Output variables include gross primary production (GPP), net ecosystem exchange (NEE), autotrophic respiration (R_a), maximum
leaf area index (LAI_{max}), latent heat flux (LE) and yield. Parameters are: Post-harvest leaf allocation coefficient to storage (aleafstor),
initial leaf allocation coefficient (fleafi), GDD to canopy maturity (lfmat), root allocation coefficients at the start of fruit development
(arootf) and until harvest (arootf2), GDD needed until harvest (hybgdd), maximum LAI (laimx), fraction of allocation that goes to
currently displayed growth (fcur), C:N ratios of fruits (graincn) and leaves (leafcn), specific leaf area at top of canopy (slatop), slope
of the relationship between leaf N per unit area and the maximum rate of carboxylation at 25 °C (s_vcad), and the medlyn slope of
the conductance–photosynthesis relationship (medlynslope). For more details on the parameters, see Appendix C.

3.2 Modelling results

In the following, we present the modelling results according to the initial parameterization and the updated parameters values
from the sensitivity analysis. Daily simulations or yearly sums are compared to observed biomass, yield, and LAI data as well
as ecosystem fluxes retrieved from the EC measurements aggregated to daily mean values.

3.2.1 Biomass growth and yield

The patterns in seasonal biomass allocation simulated by CLM-FruitTree show good agreement with the monthly observations
from 2010 (Fig. 4a). The beginning and end of the growing season are well captured. After bud break in the beginning of
March, biomass is primarily allocated to the vegetative organs of leaves, fine roots, and woody organs, and growth is supported
by C and N reserves until the start of fruit growth in early May. In the following months, fruit biomass grows rapidly until
harvest takes place in mid-October, following the typical sigmoidal growth curve that is well captured by the new phenology

and CN allocation. Leaf biomass peaks in early July and remains constant thereafter, with leaf offset starting later October when temperatures drop below 4 °C. Pruning is performed when the tree enters dormancy by removing 85 % of the stem biomass assimilated over the season according to the observed pruning amounts in the studied apple orchard (Zanotelli et al.,

375 2013; Zanotelli et al., 2015). From 2010 to 2012, the modelled percentage of biomass allocation to plant organs was generally in agreement with the observations (Zanotelli et al., 2015) with differences ranging between 1 and 5 % for fruits, leaves, aboveground wood, and roots (Fig. 4b). Penzel et al. (2020) stated that different studies reported biomass allocation to fruits ranging from 50 to 85 % depending on apple cultivar suggesting considerable variability in allocation coefficients. This emphasizes the benefit of a cultivar specific calibration in order to obtain realistic modelling results. On the other hand, it

380 suggests that a more general parameterization, that reflects an average apple tree, may be necessary to apply CLM-FruitTree at larger scales and across multiple cultivars.
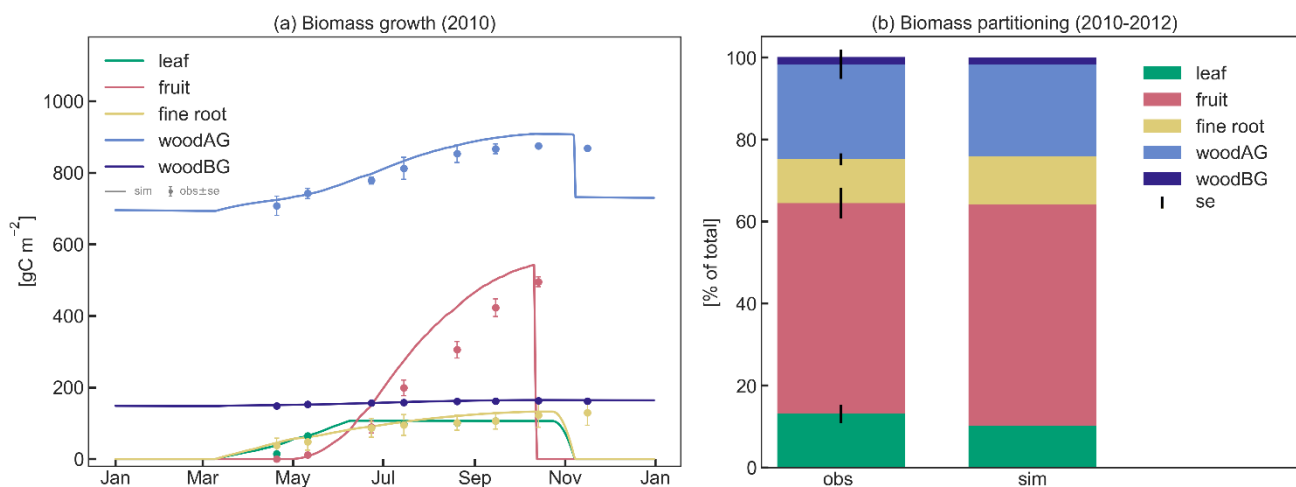

Figure 4: (a) Observed and simulated growth of leaves, fruits, fine roots, aboveground (live and dead stem), and belowground biomass (live and dead coarse roots) during 2010. (b) Observed and simulated biomass components between 2010 and 2012 as
385 **percentage of total biomass.**

The timing for initial leaf development in spring and leaf offset in late autumn are sufficiently well captured by the implemented bud burst prediction algorithm and the simple temperature threshold for leaf abscission respectively (Fig. 5). Observed maximum LAI varied between 2.8 and 3.3 m^2 m^{-2} and occurred during the first half of July. The simulations reached similar values in 2010 and 2012 matching the observations, while the lower simulated LAI in 2011 underestimated

390 measurements due to a smaller C transfer from storage and lower solar radiation early in the growing season. Such discrepancy could be further related to a light pruning performed in the previous winter (Zanotelli et al., 2013). Such management is performed to counteract the well-known alternate bearing behaviour of the Fuji apple, which causes a substantial drop in yield following a high yielding year (Belleggia et al., 2009; Atay et al., 2013; Pasa et al., 2021). In consequence to the light pruning, a larger amount of vegetative and flower buds remained on the tree leading to a higher yield and, possibly explaining the larger

395 discrepancy between relatively high observed LAI and relatively low simulated values. Measured LAI showed a slow decline

soon after maximum LAI was reached, while simulated values in contrast are assumed to remain constant until the leaf-offset period is initiated. The observed early decline may be an artefact of the sampling strategy used to determine LAI that extrapolated individual leaf area measurements to the whole tree, assuming a constant leaf distribution within the tree (Zanotelli et al., 2013). Another reason could be a limited leaf fall occurring during the summer at the expense of the inner shadowed

400   leaves, as noted during field sampling. Other studies suggest that the LAI of fruit trees generally stays constant until a rapid decline with the onset of senescence (Lakso et al., 1999; Pallas et al., 2016), supporting the simulated LAI dynamic.
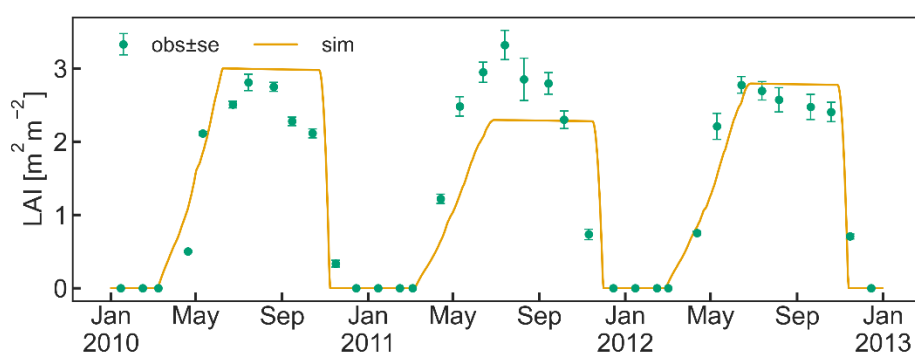

Figure 5: Observed (±standard error) and simulated leaf area index (LAI) between 2010 and 2012.

405   Simulated yield averaged at 70 t ha^{-1} between 2010 and 2015 and was within 2.3 % of the observed average yield. While simulated yield varied between 61 and 76 t ha^{-1}, the observations showed a greater inter-annual variability, as exemplified in the case of the year 2012 (low yield of 51 t ha^{-1}) and 2015 (high yield of 101 t ha^{-1}) (Fig. 6). Low inter-annual variability of yield has also been observed in previous crop simulations with CLM5 for winter wheat (Boas et al., 2021) suggesting that additional drivers of yield variability such as specific management practices are not represented with sufficient detail in CLM5.

410   In the case of apple trees, yield is tightly linked to the number of flowers and early fruit growth, which in turn depend on a complex interaction of the environmental conditions during winter dormancy and the start of the new growing season (Chmielewski et al., 2012; Corelli-Grappadelli and Lakso, 2002). Additionally, C reserves accumulated in the previous year (Greer et al., 2002) and crop load management play an important role in determining the final harvest (Penzel et al., 2020). The latter includes pruning or fruit thinning to ensure optimal fruit growth and prevent alternate bearing. The low observed

415   yield in 2012 may be a result of such behaviour. Storage growth is considered in CLM-FruitTree and exhibited an impact on the final yield of the following season as shown by the sensitivity analysis of the *aleafstor* and *fcur* parameters (Fig. 3). However, its effect on fruit growth in CLM-FruitTree is indirect since it supports leaf development in the early growth stage but does not directly contribute to fruit growth. Identifying the driving forces of reserve deposition and mobilization, and their quantification remains an unsolved issue and there is yet no consistent formulation of this process in tree modelling (Le Roux

420   et al., 2001; Allen et al., 2005). Predicting final yield in fruit orchards is further complicated by the fact that harvest is usually based on certain fruit quality traits such as firmness, or soluble solids and can occur successively as fruits may not mature at

the same time (Corelli-Grappadelli and Lakso, 2002; Musacchi and Serra, 2018). Within this context, the proposed simplifications of the C reserve dynamics and fruit harvest are likely reasons for the difference in observed and simulated yields while the missing representation of specific crop load management practices regarding the Fuji apple contributed to the low variability in simulated yields. Considering the many specific challenges in modelling this apple cultivar, we believe that the yield predictions are satisfactory enough in the context of the sub-model development.
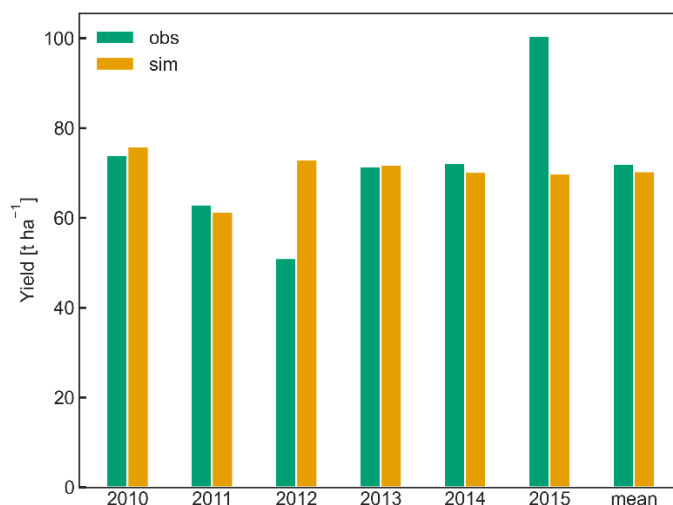

Figure 6: Annual yields from 2010 to 2015 and their mean in tons of fresh weight per hectare. For the conversion of simulated fruit biomass in gram carbon per square metre to tons per hectare, fruit C content was assumed 42 % of total dry weight, harvest efficiency was assumed 95 %, and fruit water content 83 % according to Zanotelli et al. (2013).

3.2.2 Ecosystem fluxes and soil moisture variation

Carbon fluxes

As shown in Fig. 7, CLM-FruitTree was able to capture the overall patterns of GPP, NEE, and R_{eco}, particularly during the transition between dormancy periods and growing seasons (April to November). Simulated C fluxes are highly correlated with observations ($r \geq 0.84$) while the RMSE ranges between 1.12 and 1.53 gC m^{-2} d^{-1}. Observed and simulated peak C fixation occurred mid-July (Fig. 7a), corresponding to the maximum (negative) NEE (Fig. 7c) and maximum LAI (Fig. 5). Simulated NEE becomes negative (net carbon sink) around April and returns positive (net carbon source) around November in agreement with the observed dynamic (Fig. 7c). Observed yearly sums of GPP (NEE) were 1.60 (-0.49), 1.43 (-0.48), and 1.65 (-0.76) kgC m^{-2} yr^{-1} for 2013, 2014, and 2015, respectively. Simulated yearly sums of GPP (NEE) were 1.58 (-0.53), 1.56 (-0.51), and 1.53 (-0.57) kgC m^{-2} yr^{-1} for the same years showing a negligible positive bias of on average 0.17 % for GPP (Fig. 7b) and a small underestimation (less negative) of on average 3.8 % for NEE (Fig. 7d). Simulated and observed R_{eco} (Fig. 7e) generally increased until July, because of the increase in air temperature and respiratory costs of the developing canopy, and declined thereafter as air temperature started to drop. Simulations of R_{eco} tend to slightly underestimate observations between April and late August and to overestimate observations during winter, although discrepancies are relatively small. Observed yearly sums

445 of R_{eco} were 1.13 (2013), 0.98 (2014), and 0.94 (2015) kgC m^{-2} yr^{-1} while simulated values were 1.08, 1.08, and 0.99 kgC m^{-2} yr^{-1}, respectively. CLM-FruitTree overestimated yearly R_{eco} by on average 3.3 % explaining most of the difference in observed and simulated NEE in 2013, while differences in 2014 and 2015 are owed to a combination of small biases in both GPP and R_{eco}. Measured R_{eco} showed irregular fluctuations in the early part of the growing season 2013, and mid- to late-season 2014 and 2015 that are not reproduced well by the model. These fluctuations mostly correspond to the observed temperature

450 dynamics (not shown) as a result of the applied gap filling that is based on an air (or soil) temperature-R_{eco} relationship (Reichstein et al., 2005). Such discrepancies between observed and simulated dynamics could be further explained by the occurrence of field management practices such as mowing of the grassed alleys or soil tillage under the tree rows, which are currently not represented in CLM-FruitTree. Such practices could have led to a temporary rise in soil respiration (R_s) due to increased heterotrophic respiration (R_h) as discussed in Zanotelli et al. (2013). Indeed soil tillage experiments performed in an

455 apple orchard located in a Loess plateau in Shaanxi Province in China were found to increase R_s 14-57 % depending on the tillage method (Hou et al., 2021).

Zanotelli et al. (2013) measured a total R_s of 801±95 gC m^{-2} in 2010 contributing around 90 % to R_{eco}, based on soil chamber measurements within the orchard (total soil respiration). The comparison with parallel measurements in a trenched plot produced a high ratio R_h/R_s of 0.77 for the apple orchard. In contrast, simulated R_{eco} for the same year was dominated by

460 autotrophic respiration (R_a) due to high C costs for maintenance, mainly of leaf biomass (not shown). Total simulated R_s contributed merely 45 % (510 gC m^{-2}) to R_{eco} with a ratio R_h/R_s of 0.87. Other studies found that R_s contributed 56-67 % to R_{eco} in irrigated citrus orchards of different ages (Martin-Gorriz et al., 2020) and >60 % in forest ecosystems where the magnitude of ecosystem fluxes is generally comparable to orchards (Lasslop et al., 2012; Zanotelli et al., 2013).

In addition to the missing representation of certain management practices, CLM-FruitTree currently does not account for an

465 active ground cover in the orchard which has shown to enhance R_s in an Italian olive orchard through increased fine root and microbial biomass (Turrini et al., 2017). Furthermore, the simplified representation of microbial activity in CLM5, through fixed respiration fractions for litter and soil organic matter pools, may limit the ability of CLM-FruitTree to accurately represent soil respiration processes. Not accounting for mycorrhizal respiration may fail to adequately represent R_{eco} of the orchard, as measurements suggested a substantial contribution of 11±6 % to total R_s in an apple orchard (Tomè et al., 2016). Lastly, biases

470 in simulated soil temperature or soil organic matter content could partially contribute to explain the above-discussed differences.

R_a in CLM5 is the sum of maintenance and growth respiration for the different plant organs as well as the C cost associated with N uptake from the soil, whereby maintenance respiration comprises the main part of R_a (78 % on average in this study). CLM5 calculates maintenance respiration based on tissue N content, temperature, and a constant base maintenance rate. This

475 however, does not account for a lower or varying maintenance cost observed in mature apple orchard canopies compared to annual crops (Bepete and Lakso, 1996; Lakso et al., 1999). It therefore seems likely that the cost for leaf maintenance for the orchard is unrealistically high in CLM-FruitTree, accounting for on average 45 % of R_a or 28 % of R_{eco}. In comparison, in citrus orchards, with an evergreen canopy, leaf respiration was found to contribute 18–20 % to annual R_{eco} (Martin-Gorriz et

al., 2020). This could also explain the lower simulated carbon use efficiency (NPP/GPP) of 0.59 compared to 0.71 found by
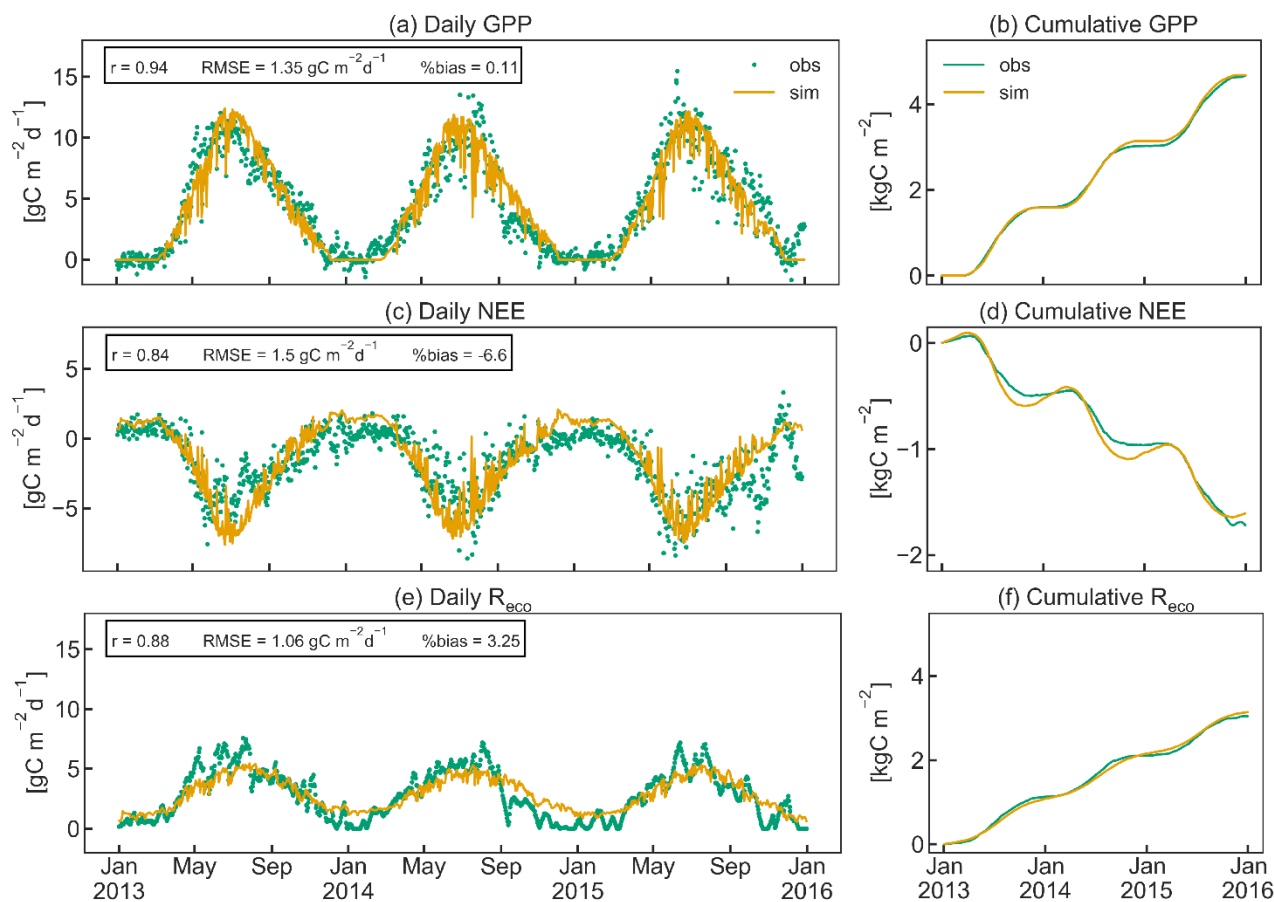480 Zanotelli et al. (2013).

Figure 7: Daily instantaneous (a, c, e) and cumulative (b, d, f) observed and simulated fluxes of gross primary productivity (GPP), net ecosystem exchange (NEE), and ecosystem respiration (R_eco) for the studied apple orchard between 2013 and 2015. Pearson's coefficient of correlation (r), the root mean square error (RMSE) and the percent bias (%bias) are displayed as statistical indices.

485 **Energy and water fluxes**

The simulated seasonal course of the energy balance components R_n, G, LE and H agrees well with observed dynamics in the orchard (Fig. 8). CLM-FruitTree shows a high performance in reproducing R_n and LE with r ≥ 0.97 and RMSE of 15.98 and 17.85 W m^{-2}, respectively (Fig. 8a and c). Due to the lack of LW_{in} measurements, the CLM5-internal LW_{in} calculation based on a clear-sky parameterization after Idso (1981) was used initially. This resulted in a significant underestimation of 5 % (511
490 MJ) for LW_{in} and 18 % (471 MJ) for R_n compared to the observations in 2010. The R_n bias could be reduced by 14 % for the observed time series when LW_{in} was calculated by considering cloud cover as described in Appendix B. This stresses the necessity to account for cloud cover, ideally combined with locally calibrated parameters, for an accurate calculation of LW_{in}. The remaining small negative bias of 4.48 % in R_n is due to negative simulated R_n during the winter months (Fig. 8b), which

may be a result of the higher reflectance of solar radiation from bare soil compared to a grass surface (Bryś et al., 2019). The
495   model assumes a bare soil (except for stem area) during the dormancy period, as the grass-covered alleys in the orchard are
not considered explicitly.

The simulated LE (Fig. 8c) shows similar dynamics and variability as the observations following the increase and decrease of
GPP (Fig. 7a) and LAI (Fig. 5). Similarly to LE, modelled ET shows a high correlation coefficient of 0.97 and small RMSE
of 0.62 mm d^{-1} (Fig. 8i). Simulated ET exceeds observed ET by 1.1 mm d^{-1} on average during its peak in July but the overall
500   bias is almost negligible (Fig. 8j). Total observed ET is 901 (2013), 858 (2014), and 883 (2015) mm while corresponding
simulated values are 916, 877, and 925 mm, respectively. When examining the order of magnitudes of the ET components,
canopy transpiration takes up around 85 % of ET, followed by soil evaporation and canopy evaporation (data not shown).
Typically, apple orchard ET represents a combined flux from the apple trees and the grassed alley system, which is not
explicitly represented in CLM-FruitTree since CLM5 does currently not consider inter-row grass coverage or intercropping.
505   Ntshidi et al. (2021) found that the contribution of understory transpiration is high in young, non-bearing apple orchards, but
contributes less than 10 % to whole orchard ET in mature orchards with high canopy cover, which may explain the good model
performance despite not considering the grass cover.

Simulated H and G are less consistent with the observations with r values of 0.54 and 0.64, respectively, and large %bias (Fig.
8e and 8g), which is partially due to the much smaller magnitudes of the two fluxes compared to R_n and LE. A possible reason
510   for the lower amplitude of observed G (Fig. 8h) compared to simulated values may be the dampening effect of the grass cover
providing additional shading during summer and insolation during winter (Bryś et al., 2019; Oorthuis et al., 2021). Observed
H was rather constant throughout the year with slightly higher values at the start and end of the growing season when the
canopy was not yet fully developed, or leaves were shedding. CLM-FruitTree simulated a clear rise of H until April, closely
following the observations, but H thereafter declined steeply in May with negative values in August 2013 and 2015. Negative
515   H during August corresponds with maximum LE and the main simulated irrigation season (June to September) that added 357
(2013), 281 (2014), and 517 mm (2015) of water to the orchard (Fig. 9a). In a study conducted with CLM4.5, intense irrigation
was found to strongly influence the convective heat fluxes by increasing LE and decreasing H (Zeng et al., 2017). Although
precise measurements of the irrigation amount in the orchard are not available for the studied period, the average yearly
irrigation was estimated around 200 mm with no irrigation in 2014 due to sufficient rainfall (Montagnani et al., 2018). The
520   difference in irrigation amounts may in part explain why the described phenomena is not observed in the measurements. Indeed
negative simulated H in the summer months occurred as a result of strong evaporative cooling of ground and vegetation
temperature through energy absorption by LE following irrigation, that caused simulated LE to exceed simulated R_n. This
behaviour was not observed in the measurements where LE rarely exceeded R_n and was mostly owed to an overestimation of
simulated LE compared to the measurements. Persisting model weaknesses in the partitioning of the energy balance were
525   pointed out by a recent study examining land surface processes over a tropical rainforest using CLM4.5 and CLM5, and were
linked to missing detail in the representation of the canopy and an oversensitivity of vegetation temperature to incoming solar
radiation among others (Song et al., 2020). As a result, the authors observed an overestimation of LE and unrealistically high

day-to-night changes in G, which was also observed in this study when examining the model output at an hourly time step (results not shown).

530   Energy partitioning in orchards is strongly influenced by the positioning and pruning of branches to optimize tree architecture for higher productivity, planting density, tree height, and LAI distribution (López-Olivari et al., 2016). Consequently, the contribution of H and LE can significantly differ in patchy compared to closed canopies of annual crops (La Fuente-Sáiz et al., 2017). Next to the aspects discussed above, biases in the simulated energy balance components are hence likely to arise from model limitations to represent such heterogeneous canopies.

Soil moisture variation

535   Simulated mean soil moisture (SM) at 5 cm depth was within 1.6 %vol of the observed value during the three observed growing seasons, despite the higher simulated irrigation amount (Fig. 9b). Simulated daily values show a greater variability than the measured data in response to precipitation and to frequent irrigation (Fig. 9a–b). In contrast, observed SM in the deeper soils (30–60 cm), was 3–11 %vol higher during the growing season compared to simulated values (Fig. 9c–d). Considering the total

540   investigated soil depth, simulations exhibit a larger variability in SM throughout the year, with a general overestimation in winter and underestimation during the growing season (especially in the deeper soils). However, the collected SM data was limited to a single soil profile that may not adequately reflect the average soil moisture of the apple orchard, which should be considered when comparing measurements and simulations. Even though the measurements are incomplete, the constant high observed SM in the deeper soils suggests an ample supply of water due to capillary rise from the shallow ground water table

545   that typically ranges between 1.2 and 1.85 m in the area (Montagnani et al., 2018). This process replenishes the water removed by ET processes and may explain the reduced need for irrigation compared to the simulations. Despite the shallow simulated ground water table (generally 1.2 m depth), groundwater could not be used for root water uptake in the simulation as the rooting depth of the orchard was restricted to 0.8 m according to local measurements and capillary rise is currently not implemented in CLM5.
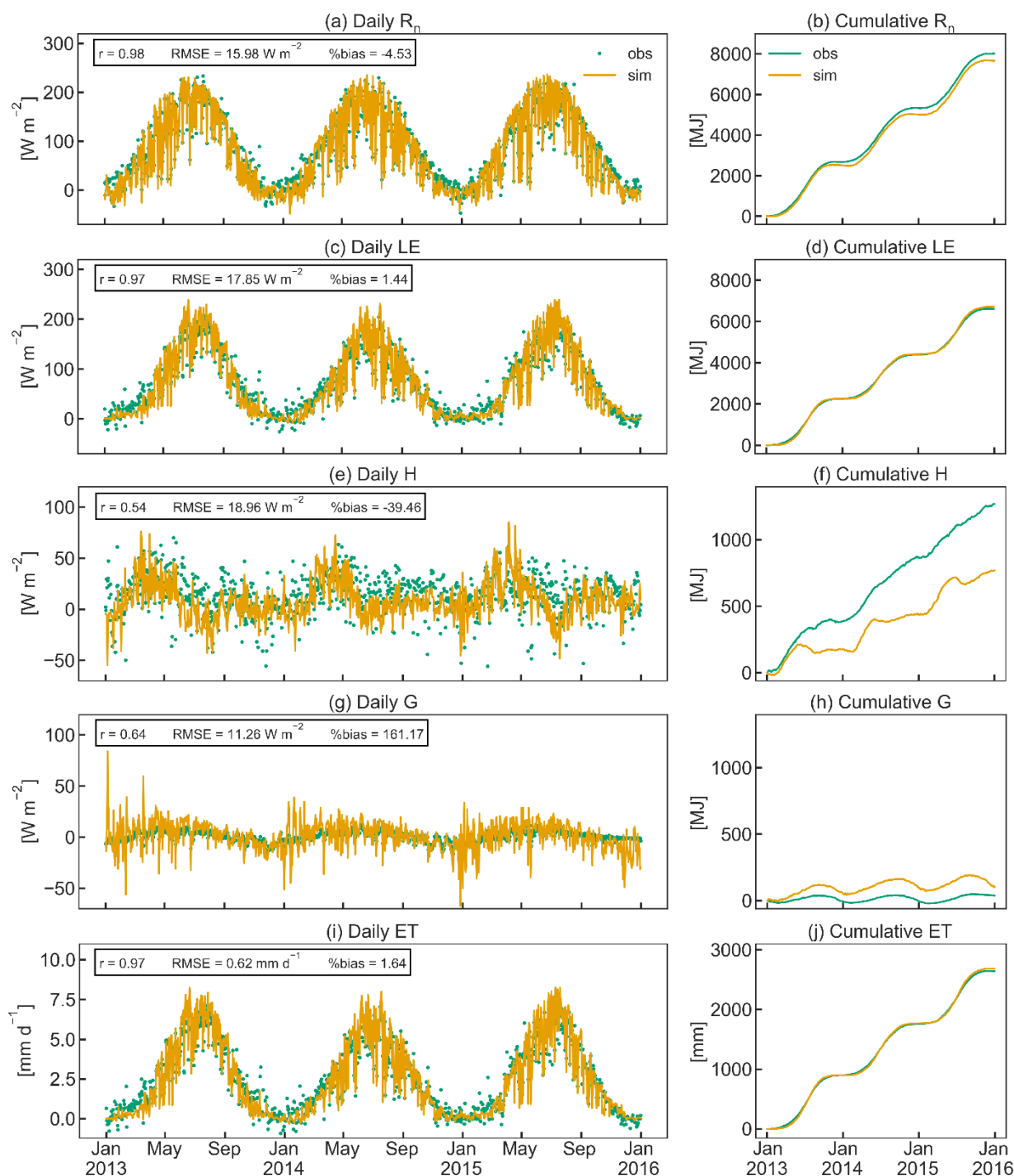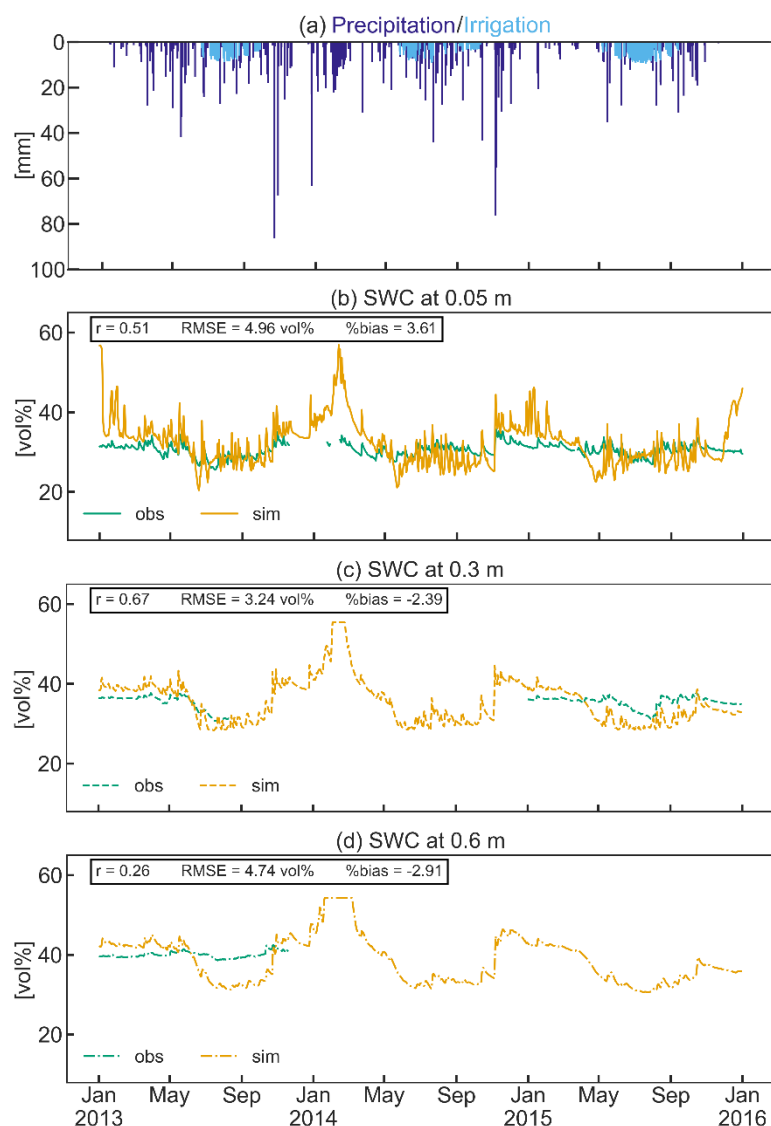
Geoscientific
Model Development
Discussions

550

Figure 8: Daily and cumulative observed and simulated fluxes of net radiation (R$_n$), ground heat (G), latent heat (H), sensible heat (LE) and evapotranspiration (ET) for the studied apple orchard between 2013 and 2015. The coefficient of determination (r), the root mean square error (RMSE) and the percent bias (%bias) are displayed as statistical indices.

23

Figure 9: Precipitation and simulated irrigation (a), and observed and simulated soil water content (SWC) at 0.05 m (b), 0.3 m (c), and 0.6 m (d) depth from 2013-2015.

4 Conclusions

The novel CLM-FruitTree was developed to model perennial deciduous fruit orchards and thus extended the representation of agricultural systems in CLM5. The development included a new phenology subroutine to account for the perennial nature, prolonged growing season, and the distinct phenological development of fruit trees compared to annual crops. Furthermore, C reserve dynamics of perennial deciduous trees were considered by adapting the CN allocation and typical management

practices associated with fruit orchards were represented, such as transplanting of seedlings and winter pruning. To evaluate the development, a new apple PFT was parameterized, and the model was set up and tested using extensive site data of a

565 mature apple orchard in Northern Italy.

One-by-one parameter sensitivity analysis revealed that photosynthetic parameters and parameters associated with canopy conductance have the highest influence on GPP, NEE, LE and yield, while phenological parameters were more influential in biomass partitioning to the different plant organs. Due to the high number of model parameters and parameter covariation, future studies could propose a more comprehensive sensitivity analysis with a training dataset consisting of multiple sites,

570 which would give more insight into model sensitivity and could further improve the parameterization.

CLM-FruitTree was able to capture the seasonal biomass development as well as the average relative partitioning of the total biomass into the different plant organs. The inclusion of C reserves next to photosynthetic growth was imperative to enable regrowth at the end of a dormancy period and influenced LAI development, total seasonal biomass, and yield. Average simulated yield was within 2.3 % of observation even though CLM-FruitTree showed a lower inter-annual variability likely

575 due to the simplification of C reserve dynamics, specific management practices, and the alternate bearing behaviour exhibited by the Fuji apple cultivar.

The new phenology and CN allocation algorithms well represented the seasonal course of carbon, water, and energy fluxes of the orchard. The magnitude of ecosystem fluxes was particularly well captured for GPP, R_n, LE, and ET with correlation coefficients > 0.94 and %bias < ±5 %. The model exhibited small biases in NEE and R_{eco} that were most likely caused by the

580 overestimation of R_a, especially leaf maintenance respiration. Possible reasons for the smaller simulated contribution of R_s to R_{eco} could be the missing representation of the grass-covered alleys, differences in simulated and actual soil temperature or organic matter content, and oversimplification of microbial respiration processes. Additionally, large negative biases in simulated H were found over most of the main irrigation season during summer as the model simulated a strong evaporative cooling of the surface temperature.

585 Further model developments should consider the improvement of canopy processes related to energy partitioning and the inclusion of an active ground cover in the orchard representation to improve the yearly energy budget calculations and possibly soil respiration. An explicit representation of the microbial community and a more flexible calculation of R_a, i.e. considering tissue age, should also be the focus of future model improvements. In addition, management practices such as mowing or soil tillage could further enhance the model capability of capturing the dynamics and fate of assimilated C. Finally, the application

590 of the newly developed sub-model to different geographical regions and other types of fruit trees or apple cultivars is needed to further validate the model and give more insight into the transferability of the development to different types of orchards.

Overall, our results demonstrate the ability of the newly developed CLM-FruitTree sub-model to represent the seasonal dynamics and magnitudes of growth and ecosystem fluxes in a deciduous fruit orchard. As such, this development constitutes an important contribution towards a more comprehensive representation of the agricultural land surface in CLM5 by adding a

595 perennial, woody crop to the existing annual crop types. This will allow for a more realistic evaluation of land use and climate

Geoscientific
Model Development
Discussions

change effects, or water availability at regional scale such as the Mediterranean or parts of China and the US, where perennial agriculture such as fruit orchards cover large parts of the agricultural landscape.

Appendix

600 **Appendix A: Sequential model for bud burst prediction**

The bud burst prediction in CLM-FruitTree is based on the sequential model developed by Cesaraccio et al. (2004). Negative chill days (C_d) are accumulated from the 1st of November followed by positive anti-chill days (C_a) to overcome the different stages of tree dormancy, rest and quiescence. The chilling requirement (C_R) defines the threshold for the accumulation of C_d and is reached when $\sum C_d \leq C_R$. Thereafter C_a accumulation begins until $C_R + \sum C_a \geq 0$ at which bud burst occurs. The

605 accumulation of C_d and C_a on a given day is calculated from maximum (T_x) and minimum (T_n) daily air temperature as well as a temperature threshold for chill accumulation (T_C), and varies depending on five possible temperature cases that relate T_x, T_n, T_C, and 0 °C with the daily mean air temperature (Table A1). The optimal values for C_R and T_C were calibrated based on bud burst observations from 2010–2013 for the Adige site by minimizing the RMSE between observations and predicted bud burst. The optimal value for C_R was -68 while T_C was 4 °C resulting in an RMSE of 7.2 days.

610 **Table A1: Chill day (C_d) and anti-chill day (C_a) calculation for five different temperature cases relating maximum (T_x) and minimum (T_n) air temperature to the air temperature threshold (T_C) and 0 °C, T_M is the air mean temperature.**

Temperature Cases	Chill days	Anti-chill days
$0 \leq T_C \leq T_n \leq T_x$	$C_d = 0$	$C_a = T_M - T_C$
$0 \leq T_n \leq T_C < T_x$	$C_d = -\left[(T_M - T_n) - \dfrac{(T_x - T_C)^2}{2(T_x - T_n)}\right]$	$C_a = \dfrac{(T_x - T_C)^2}{2(T_x - T_n)}$
$0 \leq T_n \leq T_x \leq T_C$	$C_d = -(T_M - T_n)$	$C_a = 0$
$T_n < 0 \leq T_x \leq T_C$	$C_d = -\left[\dfrac{T_x^2}{2(T_x - T_n)}\right]$	$C_a = 0$
$T_n < 0 < T_C < T_x$	$C_d = -\dfrac{T_x^2}{2(T_x - T_n)} - \dfrac{(T_x - T_C)^2}{2(T_x - T_n)}$	$C_a = \dfrac{(T_x - T_C)^2}{2(T_x - T_n)}$

Appendix B: Calculation of incoming longwave radiation

Incoming longwave radiation (LW_{in}) can be expressed based on the Stefan Boltzmann Law as:

$$LW_{in} = \varepsilon_{eff} * \sigma * T^4 = \varepsilon_{cs} * F * \sigma * T^4 \ , \tag{B1}$$

615   where ε_{eff} is the effective emissivity that can be expressed by multiplying the clear-sky atmospheric emissivity ε_{cs} with a cloud factor F (always ≥1) that expresses the increase of LW_{in} under cloudy conditions, σ is the Stefan Boltzmann constant (5.67 x 10^{-8} W m^{-2} K^{-1}) and T is the 2m air temperature in K.

Clear-sky emissivity was obtained using the Konzelmann et al. (1994) parameterization as follows:

$$\varepsilon_{cs} = 0.23 + 0.484 * \left(\frac{e}{T}\right)^{\frac{1}{8}} ,$$ (B2)

where e is the vapour pressure in Pa at 2m.

620   Equation (B1) can be rearranged to obtain F as follows:

$$F = \frac{LW_{in}}{\varepsilon_{cs} * \sigma * T^4}$$ (B3)

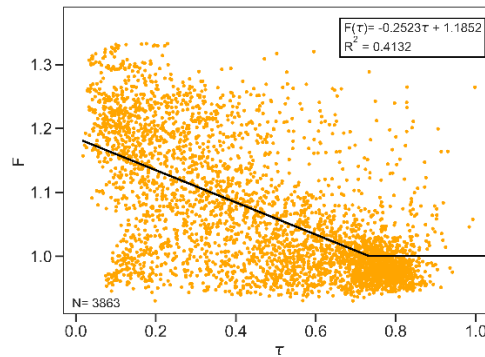F was calculated at hourly interval using measured LW_{in} data from 2010 and ε_{cs} calculated using the above Eq. (B2). As proposed by Sedlar and Hock (2009), in the absence of cloud data, the cloud factor F can be parameterized as a function of the atmospheric transmissivity index τ, which is defined as follows:

$$\tau = \frac{SW_{in}}{SW_{toa}} ,$$ (B4)

where SW_{in} is the incoming shortwave radiation, and SW_{toa} is the theoretical shortwave radiation received at the top of the
625   atmosphere.

Figure B1 shows the linear equation that was fitted to the relationship of F and τ for the year 2010. For the calculation of clear-sky emissivity, all data where τ was greater than 0.7 (N=3863) was considered based on the suggestion by Campbell (1985).

Figure B1: Cloud factor F as a function of atmospheric emissivity τ for hourly observations. The black line represents the linear
630   **equation for F(τ) and F≥1. Clear-sky emissivity is parameterized based on Konzelmann et al. (1994).**

For the nighttime values and for very low incoming shortwave radiation ($SW_{in} < 15$ W m^{-2}), τ was gap-filled with the mean of the two surrounding values to obtain a complete time series of LW_{in} data. Figure B2 shows the results of the LW_{in}

parameterization compared to LW_{in} calculated by CLM5 and to the observed data for the year 2010. As performance statistics the Pearson's r (r), the root mean square error (RMSE) and percent bias (%bias) are given.
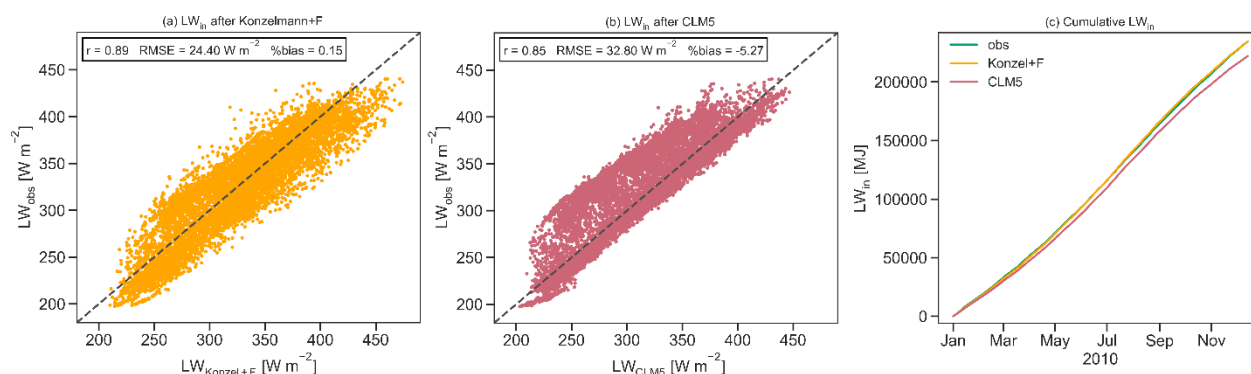

Figure B2: Comparison of observed LW_{in} with the parameterization using (a) Konzelmann et al. (1994) according to Eq. (B2) and the cloud factor parameterization F(τ), and (b) the calculation procedure used in CLM5, as well as (c) cumulative observed and calculated LW_{in} for 2010. Pearson's r, RMSE and %bias are given as performance statistics.

Geoscientific
Model Development
Discussions

Appendix C: Parameters used in CLM-FruitTree and for the apple PFT

Table C1: Parameters adapted or added in the new CLM-FruitTree sub-model and the apple PFT including phenology, CN allocation, photosynthesis, vegetation structure as well as optical and respiration parameters. Parameters were adjusted based on field observations or literature values and are listed with their definition, unit, value, and references to the literature.

Parameter	Definition	Unit	Value	Reference
Phenological parameters				
baset	Base temperature for GDD accumulation	°C	4	Based on commonly used values for apple trees (Reyes et al., 2016; Díez-Palet et al., 2019; Penzel et al., 2020)
crequ	Chilling requirements for bud burst of fruit tree crops	unitless	-68	Calibrated using bud break dates from Zanotelli et al. (2013) and Zanotelli et al. (2015), and the sequential model (Cesaraccio et al., 2004)
crit_temp	Critical temperature to initiate leaf offset for fruit tree crops	K	278.15	Adjusted based on LAI measurements (Zanotelli et al., 2013)
grnfill* (GDDfruit)	GDD needed from bud break to beginning of fruit development	°days	400	Based on observed and commonly used values for apple trees (Zanotelli et al., 2013; Lakso et al., 2000; Neumann, 2020; Penzel et al., 2020)
grnrp*(GDDripe)	GDD needed from bud break to the fruit ripening phase	°days	1100	Based on observed and commonly used values for apple trees (Lakso et al., 2000; Zanotelli et al., 2013; Neumann, 2020; Penzel et al., 2020)
huileaf (GDDleaf)	GDD accumulated at the moment of bud break (end of dormancy period)	°days	–	Calculated based on sequential model for bud burst prediction (Cesaraccio et al., 2004)
hybgdd* (GDDmat)	GDD needed from bud break until fruit harvest	°days	2880	Based on observed and commonly used values for apple trees (Lakso et al., 2000; Zanotelli et al., 2013; Neumann, 2020; Penzel et al., 2020)
laimx*	Maximum leaf area index	m^2/m^2	3	Based on observed and commonly used values for apple trees (Valancogne et al., 1999; Li et al., 2002; Zanotelli et al., 2013)
lfmat*(GDDlfmat)	GDD needed from bud break to canopy maturity	°days	1350	Based on observed and commonly used values for apple trees (Lakso et al., 2000; Zanotelli et al., 2013; Neumann, 2020; Penzel et al., 2020)

640

Parameter	Description	Units	Value	Notes
max_NH_harvest_date	maximum harvest date for northern hemisphere (NH)	date (md)	1015	Based on typical harvest dates in NH
max_NH_planting_date	maximum planting date for NH	date (md)	101	Only needed for orchard establishment and initiation of sequential model for bud break, tree is still dormant
min_NH_planting_date	minimum planting date for NH	date (md)	101	Only needed for orchard establishment and initiation of sequential model for bud break, tree is still dormant
mxmat	Maximum orchard age	days	9125	Based on common values for apple orchards (Lakso et al., 2000; Zanotelli et al., 2013; Penzel et al., 2020)
ndays_stor	Length of period for storage growth of fruit tree crops	days	50	Based on common values for fruit orchards (Kozlowski, 1992; Dejong and Grossman, 1994; Wünsche and Lakso, 2000)
perennial	Binary flag for perennial crop phenology	unitless	1	
root_dmx	Maximum rooting depth of crops	m	0.8	Based on observed rooting depth (Zanotelli et al., 2013)
rootprof_beta*	Rooting beta parameter, for C and N vertical discretization	unitless	0.964	Calibrated based on root sampling campaign of root mass up to 60cm (Zanotelli 2010, unpublished data)
woody	Binary flag for woody lifeform	unitless	1	
C and N allocation parameters				
aleaff*	Final leaf allocation coefficient	unitless	0.01	Adjusted based on monthly biomass measurements (Zanotelli et al., 2013)
aleafstor*	Leaf allocation coefficient to storage post-harvest used in CNAllocation	unitless	0.3	Adjusted based on monthly biomass measurements (Zanotelli et al., 2013)
allconss*	Power to control the shape of the stem allocation curve	unitless	1.5	Adjusted based on monthly biomass measurements (Zanotelli et al., 2013)
arootf*	Root allocation coefficient at start of fruit development	unitless	0.2	Adjusted based on monthly biomass measurements (Zanotelli et al., 2013)
arootf2*	Final root allocation coefficient until harvest	unitless	0.08	Adjusted based on monthly biomass measurements (Zanotelli et al., 2013)
arooti*	Initial root allocation coefficient	unitless	0.7	Adjusted based on monthly biomass measurements (Zanotelli et al., 2013)

Geoscientific
Model Development
Discussions

Parameter	Description	Unit	Value	Notes
astemf*	Final stem allocation coefficient]	unitless	0.22	Adjusted based on monthly biomass measurements (Zanotelli et al., 2013)
bfact*	Exponential factor used for fraction allocated to leaf	unitless	-0.5	Adjusted based on monthly biomass measurements (Zanotelli et al., 2013)
declfact*	Decline factor to control the shape of the stem allocation curve	unitless	4	Adjusted based on monthly biomass measurements (Zanotelli et al., 2013)
fcur*	Fraction of C and N allocated to the displayed pools	unitless	0.95	Tuned based on observed LAI and yield data (Zanotelli et al., 2013)
fleafi*	Initial leaf allocation coefficient	unitless	0.85	Adjusted based on monthly biomass measurements (Zanotelli et al., 2013)
flivewd	Fraction of new wood that is live		0.15	Same as BDT in CLM5
frootCN	Fine root C:N ratio	gC/gN	32	Average of 6 measurements (Zanotelli 2010, unpublished data)
grainCN*	Fruit C:N ratio	gC/gN	139	Average of 6 measurements (Zanotelli 2010, unpublished data)
leafCN*	Leaf C:N ratio	gC/gN	19.7	Average of 6 measurements (Zanotelli 2010, unpublished data)
lflitCN	Litter C:N ratio	gC/gN	60	Average of 4 measurements (Zanotelli 2010, unpublished data)
livewdCN	Livewood C:N ratio	gC/gN	60	Average of 6 measurements (Zanotelli 2010, unpublished data)
transplant	Initial carbon for crops transplanted from nursery	gC	5	
Photosynthetic parameters				
i_vcad*	Intercept of the relationship between leaf N per unit area and Vcmax25top	$\mu molCO_2/m^2/s$	5.2	Adjusted in between BDT and crop
medlynslope*	Medlyn slope of conductance–photosynthesis relationship	$\mu molH_2O/\mu molCO_2$	8.2	Tuned based observed GPP and ET data (Zanotelli et al., 2015)
s_vcad*	Slope of the relationship between leaf N per unit area and Vcmax25top	$\mu molCO_2/s/gN$	34	Tuned based on observed LAI and yield data (Zanotelli et al., 2013)
slatop*	Specific leaf area at top of canopy	m^2/gC	0.028	Mean value for the growing season based on LAI and leaf biomass measurements (Zanotelli et al., 2013)

Vegetation structure and management

Parameter	Description	Units	Value	Source
displar	Ratio of displacement height to canopy top height	unitless	0.67	Same as BDT in CLM5
mulch_pruning	Binary flag for mulching (1) or export (0) of pruning material	unitless	1	Based on reported organic farming practices (Zanotelli et al., 2013)
prune_fr	Fraction of dead stem that is pruned	unitless	0.85	Based on reported pruning quantity (Zanotelli et al., 2015)
stocking	Number of trees per hectare	trees/ha	3333	Based on reported planting density (Zanotelli et al., 2013)
taper	Ratio of stem height to radius at breast height	unitless	120	Based on reported stem diameter and tree height (Zanotelli et al., 2013)
xl*	Leaf/stem orientation index	unitless	0.25	Same as BDT in CLM5
z0mr*	Ratio of momentum roughness length to canopy top height	unitless	0.06	Based on average values reported for apple (La Fuente-Sáiz et al., 2017) and citrus (Tanny and Cohen, 2003) orchards
ztopmx	Maximum canopy height for crops	m	4	Based on reported tree heights (Zanotelli et al., 2013)

Optical parameters

Parameter	Description	Units	Value	Source
rholnir*	Leaf reflectance: near-IR	fraction	0.5	Based on average values for apple trees (Bastías and Corelli-Grappadelli, 2012)
rholvis*	Leaf reflectance: visible	fraction	0.1	Based on average values for apple trees (Bastías and Corelli-Grappadelli, 2012)
rhosnir*	Stem reflectance: near-IR	fraction	0.39	Same as BDT in CLM5
rhosvis*	Stem reflectance: visible	fraction	0.16	Same as BDT in CLM5
taulnir*	Leaf transmittance: near-IR	fraction	0.3	Based on average values for apple trees (Bastías and Corelli-Grappadelli, 2012)
taulvis*	Leaf transmittance: visible	fraction	0.04	Based on average values for apple trees (Bastías and Corelli-Grappadelli, 2012)
tausnir*	Stem transmittance: near-IR	fraction	0.001	Same as BDT in CLM5
tausvis*	Stem transmittance: visible	fraction	0.001	Same as BDT in CLM5

Respiration

Geoscientific
Model Development
Discussions

| FUN_fracfixers* | The maximum fraction of assimilated carbon that can be used to pay for N fixation | fraction | 0.25 | Same as BDT in CLM5 |
| lmr_intercept_atkin | Intercept in the calculation of the top of canopy leaf maintenance respiration base rate. | $\mu molCO_2/m^2/s$ | 1.756 | Same as BDT in CLM5 |

* parameters included in the sensitivity analysis

Geoscientific
Model Development
Discussions

References

Aguilera, E., Guzmán, G., and Alonso, A.: Greenhouse gas emissions from conventional and organic cropping systems in Spain. II. Fruit tree orchards, Agronomy for Sustainable Development, 35, 725-737, https://doi.org/10.1007/s13593-014-0265-y, 2015.

660 Allen, M., Prusinkiewicz, P., and DeJong, T.: Using L-systems for modeling source–sink interactions, architecture and physiology of growing trees: the L-PEACH model, New phytologist, 166, 869-880, https://doi.org/10.1111/j.1469-8137.2005.01348.x, 2005.

Anderson, J., Richardson, E., and Kesner, C.: Validation of chill unit and flower bud phenology models for 'Montmorency' sour cherry, I International Symposium on Computer Modelling in Fruit Research and Orchard Management 184, 71-78, https://doi.org/10.17660/ActaHortic.1986.184.7, 1985.

665 Atay, A. N., Koyuncu, F., and Atay, E.: Relative susceptibility of selected apple cultivars to alternate bearing, Journal of Biological and Environmental Sciences, 7, 81-86, 2013.

Balsamo, G., Beljaars, A., Scipal, K., Viterbo, P., van den Hurk, B., Hirschi, M., and Betts, A. K.: A revised hydrology for the ECMWF model: Verification from field site to terrestrial water storage and impact in the Integrated Forecast System, Journal of hydrometeorology, 10, 623-643, https://doi.org/10.1175/2008JHM1068.1, 2009.

670 Bastías, R. M. and Corelli-Grappadelli, L.: Light quality management in fruit orchards: physiological and technological aspects, Chilean Journal of Agricultural Research, 72, 574, 2012.

Belleggia, A., Murri, G., and Neri, D.: Crop load control of 'Fuji' apple in central Italy, XI International Symposium on Plant Bioregulators in Fruit Production 884, 399-405, https://doi.org/10.17660/ActaHortic.2010.884.48, 2009.

Benyei, P., Cohen, M., Gresillon, E., Angles, S., Araque-Jiménez, E., Alonso-Roldán, M., and Espadas-Tormo, I.: Pruning waste
675 management and climate change in Sierra Mágina's olive groves (Andalusia, Spain), Regional environmental change, 18, 595-605, https://doi.org/10.1007/s10113-017-1230-5, 2018.

Bepete, M. and Lakso, A.: Apple fruit respiration in the field: relationships to fruit growth rate, temperature, and light exposure, VI International Symposium on Integrated Canopy, Rootstock, Environmental Physiology in Orchard Systems 451, 319-326, https://doi.org/10.17660/ActaHortic.1997.451.37, 1996.

680 Blyth, E. M., Arora, V. K., Clark, D. B., Dadson, S. J., De Kauwe, M. G., Lawrence, D. M., Melton, J. R., Pongratz, J., Turton, R. H., and Yoshimura, K.: Advances in land surface modelling, Current Climate Change Reports, 7, 45-71, https://doi.org/10.1007/s40641-021-00171-5, 2021.

Boas, T., Bogena, H., Grünwald, T., Heinesch, B., Ryu, D., Schmidt, M., Vereecken, H., Western, A., and Hendricks Franssen, H.-J.: Improving the representation of cropland sites in the Community Land Model (CLM) version 5.0, Geoscientific Model Development,
685 14, 573-601, https://doi.org/10.5194/gmd-14-573-2021, 2021.

Bollard, E.: Transport in the xylem, Annual Review of Plant Physiology, 11, 141-166, 1960.

Bryś, K., Bryś, T., and Ojrzyńska, H.: Long-wave radiation balances of grassy surface and bare soil in Wrocław, E3S Web of Conferences, 1-8, https://doi.org/10.1051/e3sconf/201911600012, 2019.

Bwalya, J. M.: Estimation of net carbon sequestration potential of citrus under different management systems using the life cycle approach,
690 M.S. thesis, University of Zambia, http://thesisbank.jhia.ac.ke/id/eprint/8503, 2012.

Campbell, G. S.: Soil physics with BASIC: transport models for soil-plant systems, Elsevier, Washington, U.S., 1985.

Carranca, C., Brunetto, G., and Tagliavini, M.: Nitrogen nutrition of fruit trees to reconcile productivity and environmental concerns, Plants, 7, 1-12, https://doi.org/10.3390/plants7010004, 2018.

695 Cesaraccio, C., Spano, D., Snyder, R. L., and Duce, P.: Chilling and forcing model to predict bud-burst of crop and forest species, Agricultural and Forest Meteorology, 126, 1-13, https://doi.org/10.1016/j.agrformet.2004.03.002, 2004.

Cheng, Y., Huang, M., Chen, M., Guan, K., Bernacchi, C., Peng, B., and Tan, Z.: Parameterizing perennial bioenergy crops in Version 5 of the Community Land Model based on site-level observations in the Central Midwestern United States, Journal of Advances in Modeling Earth Systems, 12, 1-24, https://doi.org/10.1029/2019MS001719, 2020.

Chmielewski, F.-M., Blümel, K., and Pálešová, I.: Climate change and shifts in dormancy release for deciduous fruit crops in Germany, 700 Climate research, 54, 209-219, https://doi.org/10.3354/cr01115, 2012.

Corelli-Grappadelli, L. and Lakso, A. N.: Fruit development in deciduous tree crops as affected by physiological factors and environmental conditions (keynote), XXVI International Horticultural Congress: Key Processes in the Growth and Cropping of Deciduous Fruit and Nut Trees 636, 425-441, https://doi.org/10.17660/ActaHortic.2004.636.52, 2002.

Corelli-Grappadelli, L. and Marini, R.: 11 Orchard Planting Systems, in: The peach: botany, production and uses, CABI, Pennsylvania, U.S., 705 264, 2008.

Dagon, K., Sanderson, B. M., Fisher, R. A., and Lawrence, D. M.: A machine learning approach to emulation and biophysical parameter estimation with the Community Land Model, version 5, Advances in Statistical Climatology, Meteorology and Oceanography, 6, 223-244, https://doi.org/10.5194/ascmo-6-223-2020, 2020.

DeJong, T. M. and Grossman, Y. L.: A supply and demand approach to modeling annual reproductive and vegetative growth of deciduous 710 fruit trees, HortScience, 29, 1435-1442, 1994.

Díez-Palet, I., Funes, I., Savé, R., Biel, C., de Herralde, F., Miarnau, X., Vargas, F., Àvila, G., Carbó, J., and Aranda, X.: Blooming under Mediterranean climate: Estimating cultivar-specific chill and heat requirements of almond and apple trees using a statistical approach, Agronomy, 9, 760-781, https://doi.org/10.3390/agronomy9110760, 2019.

Dombrowski, O.: odombro/CTSM: CLM-FruitTree: A new sub-model for deciduous fruit trees, Zenodo, 715 https://doi.org/10.5281/zenodo.6025014, 2022.

El Jaouhari, N., Abouabdillah, A., Bouabid, R., Bourioug, M., Aleya, L., and Chaoui, M.: Assessment of sustainable deficit irrigation in a Moroccan apple orchard as a climate change adaptation strategy, Science of the total environment, 642, 574-581, https://doi.org/10.1016/j.scitotenv.2018.06.108, 2018.

Fader, M., von Bloh, W., Shi, S., Bondeau, A., and Cramer, W.: Modelling Mediterranean agro-ecosystems by including agricultural trees 720 in the LPJmL model, Geoscientific Model Development, 8, 3545-3561, https://doi.org/10.5194/gmd-8-3545-2015, 2015.

Fan, Y., Roupsard, O., Bernoux, M., Le Maire, G., Panferov, O., Kotowska, M. M., and Knohl, A.: A sub-canopy structure for simulating oil palm in the Community Land Model (CLM-Palm): phenology, allocation and yield, Geoscientific Model Development, 8, 3785-3800, https://doi.org/10.5194/gmd-8-3785-2015, 2015.

FAO Crops and livestock products: https://www.fao.org/faostat/en/#data/QCL, last access: 22 December 2021.

725 Faust, M., Erez, A., Rowland, L. J., Wang, S. Y., and Norman, H. A.: Bud dormancy in perennial fruit trees: physiological basis for dormancy induction, maintenance, and release, HortScience, 32, 623-629, 1997.

Fisher, R. A. and Koven, C. D.: Perspectives on the future of land surface models and the challenges of representing complex terrestrial systems, Journal of Advances in Modeling Earth Systems, 12, 1-24, https://doi.org/10.1029/2018MS001453, 2020.

Glover, J. D., Reganold, J., Bell, L., Borevitz, J., Brummer, E., Buckler, E. S., Cox, C., Cox, T. S., Crews, T., and Culman, S.: Increased 730 food and ecosystem security via perennial grains, Science, 328, 1638-1639, https://doi.org/10.1126/science.1188761, 2010.

Göhler, M., Mai, J., and Cuntz, M.: Use of eigendecomposition in a parameter sensitivity analysis of the Community Land Model, Journal of Geophysical Research: Biogeosciences, 118, 904-921, https://doi.org/10.1002/jgrg.20072, 2013.

Goldschmidt, E. E. and Lakso, A. N.: Fruit tree models: scope and limitations, Information and Communication Technology (ICT) Development and Adoption: Perspectives of Technological Innovation, 1-19, 2005.

735 Grechi, I., Sauge, M. H., Sauphanor, B., Hilgert, N., Senoussi, R., and Lescourret, F.: How does winter pruning affect peach tree–Myzus persicae interactions?, Entomologia Experimentalis et Applicata, 128, 369-379, https://doi.org/10.1111/j.1570-7458.2008.00720.x, 2008.

Greer, D. H., Wünsche, J. N., and Halligan, E. A.: Influence of postharvest temperatures on leaf gas exchange, carbohydrate reserves and allocations, subsequent budbreak, and fruit yield of 'Braeburn'apple (Malus domestica) trees, New Zealand Journal of Crop and 740 Horticultural Science, 30, 175-185, https://doi.org/10.1080/01140671.2002.9514213, 2002.

Hammad, H. M., Nauman, H. M. F., Abbas, F., Ahmad, A., Bakhat, H. F., Saeed, S., Shah, G. M., Ahmad, A., and Cerdà, A.: Carbon sequestration potential and soil characteristics of various land use systems in arid region, Journal of environmental management, 264, 110254, https://doi.org/10.1016/j.jenvman.2020.110254, 2020.

Heide, O. M. and Prestrud, A. K.: Low temperature, but not photoperiod, controls growth cessation and dormancy induction and release in 745 apple and pear, Tree physiology, 25, 109-114, https://doi.org/10.1093/treephys/25.1.109, 2005.

Hou, T., Wang, Y., Guo, F., Jia, Q., Wu, X., Wang, E., and Hong, J.: Soil Respiration Characteristics and Influencing Factors for Apple Orchards in Different Regions on the Loess Plateau of Shaanxi Province, Sustainability, 13, 1-21, https://doi.org/10.3390/su13094780, 2021.

750 Idso, S. B.: A set of equations for full spectrum and 8-to 14-μm and 10.5-to 12.5-μm thermal radiation from cloudless skies, Water resources research, 17, 295-304, https://doi.org/10.1029/WR017i002p00295, 1981.

Jackson, D.: Flowers and fruit, in: Temperate and subtropical fruit production., CABI, Cambridge, U.K., 34-43, 2011.

Kazimierski, P., Hercel, P., Suchocki, T., Smoliński, J., Pladzyk, A., Kardaś, D., Łuczak, J., and Januszewicz, K.: Pyrolysis of Pruning Residues from Various Types of Orchards and Pretreatment for Energetic Use of Biochar, Materials, 14, 1-14, https://doi.org/10.3390/ma14112969, 2021.

755 Konzelmann, T., van de Wal, R. S., Greuell, W., Bintanja, R., Henneken, E. A., and Abe-Ouchi, A.: Parameterization of global and longwave incoming radiation for the Greenland Ice Sheet, Global and Planetary change, 9, 143-164, https://doi.org/10.1016/0921-8181(94)90013-2, 1994.

Kozlowski, T.: Carbohydrate sources and sinks in woody plants, The botanical review, 58, 107-222, 1992.

Krinner, G., Viovy, N., de Noblet-Ducoudré, N., Ogée, J., Polcher, J., Friedlingstein, P., Ciais, P., Sitch, S., and Prentice, I. C.: A dynamic
760 global vegetation model for studies of the coupled atmosphere-biosphere system, Global Biogeochemical Cycles, 19, 1-33, https://doi.org/10.1029/2003GB002199, 2005.

la Fuente-Sáiz, D., Ortega-Farías, S., Fonseca, D., Ortega-Salazar, S., Kilic, A., and Allen, R.: Calibration of METRIC model to estimate energy balance over a drip-irrigated apple orchard, Remote Sensing, 9, 1-18, https://doi.org/10.3390/rs9070670, 2017.

Lakso, A., White, M., and Tustin, D.: Simulation modeling of the effects of short and long-term climatic variations on carbon balance of
765 apple trees, VII International Symposium on Orchard and Plantation Systems 557, 473-480, https://doi.org/10.17660/ActaHortic.2001.557.63, 2000.

Lakso, A., Wunsche, J., Palmer, J., and Grappadelli, L. C.: Measurement and modeling of carbon balance of the apple tree, HortScience, 34, 1040-1047, 1999.

Lasslop, G., Migliavacca, M., Bohrer, G., Reichstein, M., Bahn, M., Ibrom, A., Jacobs, C., Kolari, P., Papale, D., and Vesala, T.: On the
770 choice of the driving temperature for eddy-covariance carbon dioxide flux partitioning, Biogeosciences, 9, 5243-5259, https://doi.org/10.5194/bg-9-5243-2012, 2012.

Lawrence, D., Fisher, R., Koven, C., Oleson, K., Swenson, S., Vertenstein, M., Andre, B., Bonan, G., Ghimire, B., and van Kampenhout, L.: Technical description of version 5.0 of the Community Land Model (CLM), Natl. Cent. Atmospheric Res. (NCAR), available at: http://www.cesm.ucar.edu/models/cesm2/land/CLM50_Tech_Note.pdf (last access: 2 May 2021), 2018.

775 Le Roux, X., Lacointe, A., Escobar-Gutiérrez, A., and Le Dizès, S.: Carbon-based models of individual tree growth: a critical appraisal, Annals of Forest Science, 58, 469-506, https://doi.org/10.1051/forest:2001140, 2001.

Ledo, A., Smith, P., Zerihun, A., Whitaker, J., Vicente-Vicente, J. L., Qin, Z., McNamara, N. P., Zinn, Y. L., Llorente, M., and Liebig, M.: Changes in soil organic carbon under perennial crops, Global change biology, 26, 4158-4168, https://doi.org/10.1111/gcb.15120, 2020.

Li, F., Cohen, S., Naor, A., Shaozong, K., and Erez, A.: Studies of canopy structure and water use of apple trees on three rootstocks,
780 Agricultural Water Management, 55, 1-14, https://doi.org/10.1016/S0378-3774(01)00184-6, 2002.

Lobianco, A. and Roberto, E.: The regional model for Mediterranean agriculture, Munich Personal RePEc Archive (MPRA), Munich, Germany, IDEMA DELIVERABLE No. 17, 2006.

Loescher, W. H., McCamant, T., and Keller, J. D.: Carbohydrate reserves, translocation, and storage in woody plant roots, HortScience, 25, 274-281, 1990.

785 López-Olivari, R., Ortega-Farías, S., and Poblete-Echeverría, C.: Partitioning of net radiation and evapotranspiration over a superintensive drip-irrigated olive orchard, Irrigation science, 34, 17-31, https://doi.org/10.1007/s00271-015-0484-2, 2016.

Luo, Q., Wen, J., Hu, Z., Lu, Y., and Yang, X.: Parameter sensitivities of the Community Land Model at two alpine sites in the three-river source region, Journal of Meteorological Research, 34, 851-864, https://doi.org/10.1007/s13351-020-9205-8, 2020.

Maestre-Valero, J. F., Testi, L., Jiménez-Bello, M. A., Castel, J. R., and Intrigliolo, D. S.: Evapotranspiration and carbon exchange in a citrus
790 orchard using eddy covariance, Irrigation Science, 35, 397-408, https://doi.org/10.1007/s00271-017-0548-6, 2017.

Martin-Gorriz, B., González-Real, M. M., Egea, G., and Baille, A.: Ecosystem respiration of old and young irrigated citrus orchards in a semiarid climate, Agricultural and Forest Meteorology, 280, 1-15, https://doi.org/10.1016/j.agrformet.2019.107787, 2020.

Millard, P.: Ecophysiology of the internal cycling of nitrogen for tree growth, Zeitschrift für Pflanzenernährung und Bodenkunde, 159, 1-10, https://doi.org/10.1002/jpln.1996.3581590102, 1996.

795 Montagnani, L., Zanotelli, D., Tagliavini, M., and Tomelleri, E.: Timescale effects on the environmental control of carbon and water fluxes of an apple orchard, Ecology and evolution, 8, 416-434, https://doi.org/10.1002/ece3.3633, 2018.

Montanaro, G., Celano, G., Dichio, B., and Xiloyannis, C.: Effects of soil-protecting agricultural practices on soil organic carbon and productivity in fruit tree orchards, Land Degradation & Development, 21, 132-138, https://doi.org/10.1002/ldr.917, 2010.

Murneek, A. E.: Quantitative distribution of nitrogen and carbohydrates in apple trees, University of Missouri, College of Agriculture,
800 Missouri, U.S., 1-28, 1942.

Musacchi, S. and Serra, S.: Apple fruit quality: Overview on pre-harvest factors, Scientia Horticulturae, 234, 409-430, https://doi.org/10.1016/j.scienta.2017.12.057, 2018.

Neumann, L.: Improving the apple carbon balance model MaluSim by integrating and testing water deficit and fruit drop effects, M.A. thesis, Hannover: Institutionelles Repositorium der Leibniz Universität Hannover, Hannover, Germany, 147 pp., https://doi.org/10.15488/10194, 2020.

Noilhan, J. and Mahfouf, J.-F.: The ISBA land surface parameterisation scheme, Global and planetary Change, 13, 145-159, https://doi.org/10.1016/0921-8181(95)00043-7, 1996.

Ntshidi, Z., Dzikiti, S., Mazvimavi, D., and Mobe, N.: Contribution of understorey vegetation to evapotranspiration partitioning in apple orchards under Mediterranean climatic conditions in South Africa, Agricultural Water Management, 245, 1-11, https://doi.org/10.1016/j.agwat.2020.106627, 2021.

O'Connell, M. and Scalisi, A.: Sensing fruit and tree performance under deficit irrigation in 'September Bright' nectarine, International Symposium on Precision Management of Orchards and Vineyards 1314, 9-16, https://doi.org/10.17660/ActaHortic.2021.1314.2, 2019.

Oliveira, C. M. and Priestley, C. A.: Carbohydrate reserves in deciduous fruit trees, Hort. Rev, 10, 403-430, 1988.

Oorthuis, R., Vaunat, J., Hürlimann, M., Lloret, A., Moya, J., Puig-Polo, C., and Fraccica, A.: Slope orientation and vegetation effects on soil thermo-hydraulic behavior. An experimental study, Sustainability, 13, 1-14, https://doi.org/10.3390/su13010014, 2021.

Pallas, B., Da Silva, D., Valsesia, P., Yang, W., Guillaume, O., Lauri, P.-E., Vercambre, G., Génard, M., and Costes, E.: Simulation of carbon allocation and organ growth variability in apple tree by connecting architectural and source–sink models, Annals of Botany, 118, 317-330, https://doi.org/10.1093/aob/mcw085, 2016.

Pasa, M. d. S., Carra, B., Brighenti, A. F., Pinto, F. A. M. F., Mello-Farias, P. C. d., and Herter, F. G.: Ethephon as a potential tool to manage alternate bearing of 'Fuji' apple trees, Revista Ceres, 68, 180-184, https://doi.org/10.1590/0034-737X202168030003, 2021.

Penzel, M., Lakso, A. N., Tsoulias, N., and Zude-Sasse, M.: Carbon consumption of developing fruit and the fruit bearing capacity of individual RoHo 3615 and Pinova apple trees, Int. Agrophys., 34, 409-423, https://doi.org/10.31545/intagr/127540, 2020.

Prentice, I. C., Liang, X., Medlyn, B. E., and Wang, Y.-P.: Reliable, robust and realistic: the three R's of next-generation land-surface modelling, Atmospheric Chemistry and Physics, 15, 5987-6005, https://doi.org/10.5194/acp-15-5987-2015, 2015.

Reichstein, M., Falge, E., Baldocchi, D., Papale, D., Aubinet, M., Berbigier, P., Bernhofer, C., Buchmann, N., Gilmanov, T., and Granier, A.: On the separation of net ecosystem exchange into assimilation and ecosystem respiration: review and improved algorithm, Global change biology, 11, 1424-1439, https://doi.org/10.1111/j.1365-2486.2005.001002.x, 2005.

Reyes, F., DeJong, T., Franceschi, P., Tagliavini, M., and Gianelle, D.: Maximum growth potential and periods of resource limitation in apple tree, Frontiers in Plant Science, 7, 1-12, https://doi.org/10.3389/fpls.2016.00233, 2016.

Sanchez, E. E., Khemira, H., Sugar, D., and Righetti, T. L.: Nitrogen management in orchards, in: Nitrogen Fertilization in the Environment, Marcel Dekker, Inc., New York, U.S., 1995.

Scandellari, F., Caruso, G., Liguori, G., Meggio, F., Palese, A. M., Zanotelli, D., Celano, G., Gucci, R., Inglese, P., and Pitacco, A.: A survey of carbon sequestration potential of orchards and vineyards in Italy, European Journal of Horticultural Science, 81, 106-114, https://doi.org/10.17660/eJHS.2016/81.2.4, 2016.

Schaphoff, S., von Bloh, W., Rammig, A., Thonicke, K., Biemans, H., Forkel, M., Gerten, D., Heinke, J., Jägermeyr, J., and Knauer, J.: LPJmL4–a dynamic global vegetation model with managed land–Part 1: Model description, Geoscientific Model Development, 11, 1343-1375, https://doi.org/10.5194/gmd-2017-145, 2018.

Sedlar, J. and Hock, R.: Testing longwave radiation parameterizations under clear and overcast skies at Storglaciären, Sweden, The Cryosphere, 3, 75-84, https://doi.org/10.5194/tc-3-75-2009, 2009.

Segovia-Cardozo, D. A., Franco, L., and Provenzano, G.: Detecting crop water requirement indicators in irrigated agroecosystems from soil water content profiles: An application for a citrus orchard, Science of The Total Environment, 806, https://doi.org/10.1016/j.scitotenv.2021.150492, 2022.

Song, J., Miller, G. R., Cahill, A. T., Aparecido, L. M. T., and Moore, G. W.: Modeling land surface processes over a mountainous rainforest in Costa Rica using CLM4. 5 and CLM5, Geoscientific Model Development, 13, 5147-5173, https://doi.org/10.5194/gmd-13-5147-2020, 2020.

Tanny, J. and Cohen, S.: The effect of a small shade net on the properties of wind and selected boundary layer parameters above and within a citrus orchard, Biosystems Engineering, 84, 57-67, https://doi.org/10.1016/S1537-5110(02)00233-7, 2003.

Tomè, E., Ventura, M., Folegot, S., Zanotelli, D., Montagnani, L., Mimmo, T., Tonon, G., Tagliavini, M., and Scandellari, F.: Mycorrhizal contribution to soil respiration in an apple orchard, Applied Soil Ecology, 101, 165-173, https://doi.org/10.1016/j.apsoil.2016.01.016, 2016.

Tromp, J.: Nutrient reserves in roots of fruit trees, in particular carbohydrates and nitrogen, Plant and Soil, 71, 401-413, https://doi.org/10.1007/BF02182682, 1983.

Turrini, A., Caruso, G., Avio, L., Gennai, C., Palla, M., Agnolucci, M., Tomei, P. E., Giovannetti, M., and Gucci, R.: Protective green cover enhances soil respiration and native mycorrhizal potential compared with soil tillage in a high-density olive orchard in a long term study, Applied Soil Ecology, 116, 70-78, https://doi.org/10.1016/j.apsoil.2017.04.001, 2017.

Valancogne, C., Dayau, S., Pieri, P., Ferreira, M. I., Silvestre, J., and Angelocci, L.: Influence of orchard and vineyard characteristics on maximal plant transpiration, 3. International symposium on irrigation of Horticultural crops, Lisbonne, Portugal, https://hal.inrae.fr/hal-02770605, 1999.

860   Viovy, N.: CRUNCEP Version 7 - Atmospheric Forcing Data for the Community Land Model, Research Data Archive at the National Center for Atmospheric Research, Computational and Information Systems Laboratory, https://doi.org/10.5065/PZ8F-F017, 2018.

Wheaton, T., Castle, W., Whitney, J., Tucker, D., and Muraro, R.: A high density citrus planting, Proc. Fla. State Hort. Soc, Florida, U.S., 55-59, 1990.

Wu, T., Wang, Y., Yu, C., Chiarawipa, R., Zhang, X., Han, Z., and Wu, L.: Carbon sequestration by fruit trees-Chinese apple orchards as an example, PLoS one, 7, 1-13, https://doi.org/10.1371/journal.pone.0038883, 2012.

865   Wünsche, J. N. and Lakso, A. N.: Apple tree physiology-implications for orchard and tree management, Compact Fruit Tree, 33, 82-88, 2000.

Yasin, G., Farrakh Nawaz, M., Zubair, M., Qadir, I., Saleem, A. R., Ijaz, M., Gul, S., Amjad Bashir, M., Rehim, A., and Rahman, S. U.: Assessing the Contribution of Citrus Orchards in Climate Change Mitigation through Carbon Sequestration in Sargodha District, Pakistan, Sustainability, 13, 1-10, https://doi.org/10.3390/su132212412, 2021.

870   Zanotelli, D., Montagnani, L., Andreotti, C., and Tagliavini, M.: Evapotranspiration and crop coefficient patterns of an apple orchard in a sub-humid environment, Agricultural Water Management, 226, 1-11, https://doi.org/10.1016/j.agwat.2019.105756, 2019.

Zanotelli, D., Montagnani, L., Manca, G., and Tagliavini, M.: Net primary productivity, allocation pattern and carbon use efficiency in an apple orchard assessed by integrating eddy covariance, biometric and continuous soil chamber measurements, Biogeosciences, 10, 3089-3108, https://doi.org/10.5194/bg-10-3089-2013, 2013.

875   Zanotelli, D., Montagnani, L., Manca, G., Scandellari, F., and Tagliavini, M.: Net ecosystem carbon balance of an apple orchard, European Journal of Agronomy, 63, 97-104, http://dx.doi.org/10.1016/j.eja.2014.12.002, 2015.

Zavalloni, C., Andresen, J. A., and Flore, J.: Phenological Models of Flower Bud Stages and Fruit Growth ofMontmorency'Sour Cherry Based on Growing Degree-day Accumulation, Journal of the American Society for Horticultural Science, 131, 601-607, https://doi.org/10.21273/JASHS.131.5.601, 2006.

880   Zeng, Y., Xie, Z., and Liu, S.: Seasonal effects of irrigation on land–atmosphere latent heat, sensible heat, and carbon fluxes in semiarid basin, Earth System Dynamics, 8, 113-127, https://doi.org/10.5194/esd-8-113-2017, 2017.